NIST-GCR-91-597

Turbulent Upward Flame Spread for Burning Vertical Walls Made of Finite Thickness

A. K. Kulkarni
C. I. Kim
C. H. Kuo

Pennsylvania State University
Department of Mechanical Engineering
University Park, PA 16802

U.S. DEPARTMENT OF COMMERCE

NATIONAL INSTITUTE OF STANDARDS AND TECHNOLOGY

NIST

NIST-GCR-91-597

Turbulent Upward Flame Spread for Burning Vertical Walls Made of Finite Thickness

A. K. Kulkarni
C. I. Kim
C. H. Kuo

Pennsylvania State University
Department of Mechanical Engineering
University Park, PA 16802

May 1991

Issued September 1991

NIST Grant No. 60NANB8D0849

Sponsored by:
U.S. DEPARTMENT OF COMMERCE
National Institute of Standards and Technology
Building and Fire Research Laboratory
Gaithersburg, MD 20899

U.S. DEPARTMENT OF COMMERCE
Robert A. Mosbacher, Secretary
NATIONAL INSTITUTE OF STANDARDS AND TECHNOLOGY
John W. Lyons, Director

Notice

This report was prepared for the Building and Fire Research Laboratory of the National Institute of Standards and Technology under Grant Number 60NANB8D0849. The statements and conclusions contained in this report are those of the authors and do not necessarily reflect the views of the National Institute of Standards and Technology or the Building and Fire Research Laboratory.

Annual Report
for the period August 15, 1989 to August 14, 1990

on Grant No. 60NANB8D0849

TURBULENT UPWARD FLAME SPREAD FOR BURNING VERTICAL WALLS MADE OF FINITE THICKNESS

by

A.K. Kulkarni, Principal Investigator
C.I. Kim, Graduate Research Assistant
C.H. Kuo, Graduate Student

Department of Mechanical Engineering
The Pennsylvania State University
University Park, PA 16802

Submitted to Center for Fire Research
National Institute of Standards and Technology
Gaithersburg, MD 20899

May 1991

ABSTRACT

Progress made during the second year of the NIST grant number 60NANB8D0849 for the period August 15, 1989 through August 14, 1990 is reported here. This report marks the end of the first phase of the grant, for which the overall objective was to understand the basic mechanisms of upward flame spread and to develop a complete procedure to predict the flame spread on practical wall materials of finite thickness, appropriately verified by experiments. These objectives have been met. Specifically in the past year, several wall materials were tested in the upward flame spread apparatus, mathematical model development for predicting the upward flame spread was completed, and comparisons of data and predictions were made, in addition to completion of many other supporting tasks.

TABLE OF CONTENTS

ABSTRACT.....i

NOMENCLATURE.....ii

INTRODUCTION..... 1

UPWARD FLAME SPREAD EXPERIMENTS.....5

UPWARD FLAME SPREAD MODEL.....9

DISCUSSION.....15

SUMMARY AND CONCLUSIONS.....17

FIGURES.....19

APPENDIX I: Analysis of Heat Flux Measurement by Circular Foil Gages in a Mixed Convection/Radiation Environment.....55

APPENDIX II: A Generalized Correlation for Forward Heat Flux in Upward Flame Spread.....67

APPENDIX III: Time-dependent Local Mass Loss Rate of Finite-thickness Burning Walls.....72

Nomenclature

c_p = heat capacity, kJ/kg·K
D = depth of the sample, m
h_c = heat of combustion, kJ/kg
H = height of the sample, m
k = thermal conductivity, kJ/m·s·K
$\dot{m}''$ = mass loss rate per unit area, kg/m^{2}s, also a fire property
$\dot{q}''_w$ = total heat feedback to surface ahead of pyrolysis front, kW/m^2
$\dot{q}''_{wo}$ = total heat feedback at pyrolysis height, kW/m^2, also a fire property
$\dot{Q}'$ = heat release rate of line burner (igniter), kW/m
t = time, s
t_b = burnout time, s
T = temperature, K
T_{ig} = ignition (or pyrolysis) temperature, K
T_w = temperature of pyrolyzing surface, K
T_∞ = ambient temperature, K
V_p = flame spread rate, m/s
x = distance from the leading edge of the sample, m
x_b = burnout edge height, m
x_f = flame height, m
x_p = pyrolysis height, m
y = distance from the surface to the interior of the sample, m
y_w = instantaneous location of the pyrolyzing surface, m
α = heat diffusivity, m^2/s
λ = local time (time after beginning of pyrolysis), s
ρ = density, kg/m^3

ANNUAL PROGRESS REPORT

for the period August 15, 1989 to August 14, 1990

on NIST Grant No. 60NANB8D0849, titled,

UPWARD FLAME SPREAD ON A VERTICAL WALL

A.K. Kulkarni, Principal Investigator

C.I. Kim, Graduate Research Assistant

C.H. Kuo, Graduate Student

Introduction:

This annual report describes progress made during the period August 15, 1989 through August 14, 1990 on the project Upward Flame Spread on a Vertical Wall, supported under grant number 60NANB8D0849. The upward flame spread project was envisioned to be conducted in two major phases: first, a study of flame spread for practical materials of finite thickness in the absence of external radiation, and second, a study of flame spread and evaluation of indepth radiation absorption properties of materials under surrounding fire conditions, i.e., with strong external radiation. This report marks the end of the first phase which began in August 1988 and ended in August 1990, although some preliminary experimental and theoretical work on upward flame spread was also conducted earlier at NIST during January 1988 through August 1988 while Dr. Kulkarni was on a sabbatical leave from Penn State to NIST.

The overall objective of the first phase of the project was to understand the basic mechanisms of upward flame spread and to develop a complete procedure to predict the flame spread on practical wall materials of finite thickness, appropriately verified by experiments. Specifically, the study involved (i) design and fabrication of an experimental setup to study upward flame spread, (ii) measurement of heat feedback from flames to the yet-unburnt surface ahead of the pyrolysis front (or simply, the forward heat flux), (iii) correlation of the heat flux data for further modeling

purposes, (iv) measurement of upward flame spread rate of the flame tip and the pyrolysis front, (v) development of a suitable mathematical model to predict upward flame spread, (vi) identification, and if necessary, measurement, of "fire properties" of practical materials for use in the model, and (vii) comparison of data with predictions and model revisions.

The above objectives have been met and the first phase of the project has been completed in the last two years. Progress made in the first year was reported in the last annual report which is available as NIST Report No. NIST-GCR-90-584. Major milestones achieved in the past (second) year are:

(i) Several additional materials were tested in the upward flame spread apparatus. Measurements for flame height, pyrolysis height, and forward heat flux, $\dot{q}''_w(x,t)$ were made and processed.

(ii) Mathematical model development was completed for predicting upward flame spread on practical materials.

(iii) Development of a generalized correlation for heat feedback from flames, which is used in the upward flame spread model, was completed.

(iv) Comparisons of flame spread data and predictions were made.

Details on the individual tasks accomplished are given in the following sections. Activities related to publications, presentations, and theses related to the grant are summarized below.

Publications and Presentation Activities :

Kulkarni, A.K. and S. Fischer. Upward Flame Spread on Vertical Walls: Model and Experiments. Presented at the III International Seminar on Fires. Alma-Alta, USSR, September 13-17, 1989, Published in conference proceedings.

Kulkarni, A.K. Radiative and Total Heat Feedback from Flames to Surface in Vertical Wall Fires. Submitted to Experimental Heat Transfer (an International Journal), March 1990. (This was later published in vol. 3, pp. 411-426, 1990).

Kim, C.I. and A.K. Kulkarni. A Numerical Model for Upward Flame Spread, presented at the 1989 Fall Technical Meeting, Eastern Section of The Combustion Institute, Albany, NY, October 30, 31 and November 1, 1989, Published in conference proceedings.

Kim, C.I. and A.K. Kulkarni. Upward Flame Spread on Vertical Walls (A Presentation to the Sponsor), Annual Conference on Fire Research, Center for Fire Research, National Institute of Standards and Technology, Gaithersburg, MD, November 6-9, 1989.

Kulkarni, A.K. and C.I. Kim. Heat Loss to the Interior of a Free Burning Vertical PMMA Slab and its Influence on Estimation Heat of Pyrolysis. Submitted to and accepted by Combustion Science and Technology, 1989. (Later published in vol. 73, pp 493-504, 1990).

Kulkarni, A. K. and S. Fischer. Upward Flame Spread on Vertical Walls: An Approximate but Complete Model and Experiments. Presented at the ASME Winter Annual Meeting, San Francisco, CA, December 10-15, 1989, Heat Transfer in Combustion Systems, HTD Vol. 122 pp. 53-61, 1989.

Presented work in progress at an informal Workshop on Upward Flame Spread held at NIST, February 1990.

Kuo, C.H. and A.K. Kulkarni. Correction of Heat Flux Measurements by Circular Foil Gage in Mixed Convection/Radiation Environments of Wall Fires, submitted to 1991 ASME/JSME Joint Thermal Energy Conference. (Later accepted for publication in the Journal of Heat Transfer).

Kim, C.I. and A.K. Kulkarni, Upward Flame Spread on Vertical Walls of Finite Thickness, prepared for (later accepted for poster session at) the Third International Symposium on Fire Safety Science.

Kulkarni, A.K., C.I. Kim, and H.E. Mitler, Time-Dependent Local Mass Loss Rate of Finite-Thickness Burning Walls. Manuscript prepared for future publication. (Currently under review for 1991 ASME Winter Annual Meeting.)

Theses:

Kim, C. I., Upward Flame Spread on Vertical Walls, Ph. D. Thesis in Progress.

Kuo, C. H., Analysis and Calibration of Circular Foil Type Heat Flux Transducers, M.S. Paper, May 1990.

Upward Flame Spread Experiments

In the past year, we tested several materials in the upward flame spread apparatus in addition to cardboard, for which the results were reported in the last annual report. The additional materials tested are: Masonite, Black PMMA, Clear PMMA, Red Velour (textile material), Polyurethane Foam, and White Pine (wood).

Details on the upward flame spread apparatus and experiments were given in the last annual report, and therefore, are not repeated here, except for the schematic of the apparatus which is shown in Figure 1a.

Figure 1b shows a sample data set for flame height, x_f, and pyrolysis height, x_p, as a function of time after the igniter is placed at the foot of the sample. The flame height is obtained using video recording. Approximately ten readings of flame height are made over a period of 0.3 second from still frames on a TV monitor and the average, maximum, and minimum values are calculated. The data indicate that the fluctuations in the flame height increase from approximately ±5 cm at ignition when $x_f \approx 35$ cm to ±15 cm when x_f was about 1.75 m. The pyrolysis height was measured by indicating the pyrolysis edge periodically using a stick by visual inspection during the test run, which was then recorded on video and read on a monitor.

A separate test was conducted to check if there was any dependence of the video camera shutter speed on the measurement of x_f for a fixed height flame. Flames of the igniter (line burner) at a constant fuel flow rate were recorded using a range of video camera shutter speeds as shown in Figure 1c. It was found that the shutter speed does not affect the readings up to 1/1000 s; below 1/1000 s the recorded intensity of flames drops too much to obtain consistent readings. Therefore, subsequent x_f readings were taken using a speed of 1/250 s.

Figure 1d shows a sample data set for the total heat feedback measured at various fixed distances from the leading edge using Gardon (circular foil) gages. The gages were cooled using hot water at 56.7±0.7°C.

Calibration procedure for the gages was described in detail in the last annual report. A separate analytical study was conducted to evaluate the performance of the gages in a mixed radiative/convective environment; it is included in this report as Appendix I. The data of Figure 1d are replotted in Figure 1e after normalizing the distance by flame height. Best curve fit of the form $y=a_0 10^{a_1 x}$ and the correlation coefficients are also shown in that figure. These data are later used to generate a general form for the heat feedback,

$$\dot{q}''_w(x,t) = \dot{q}''_{wo}\ g\ \{ x_b(t), x_p(t), x_f(t), x \} \qquad (1)$$

Additional details on this topic are given in Appendix II.

Flame Spread Results:

Flame height and pyrolysis height vs. time data for black PMMA, clear PMMA, masonite, cardboard, polyurethane foam, white pine, and red velour textile are shown in Figures 2 through 9. Both black and clear polymethylmethacrylate slabs offered very little resistance to flame spreading. The flame height was almost constant up to 40 s because the material had not started pyrolyzing and flames were entirely from the gas burner. Flames spread quickly to the top and the results are almost identical for black and clear PMMA. This is expected since the differences between black and clear PMMA samples are minor, except for the thickness and the absorption of radiation in the visual range. Since the sample height was limited to 1.2 m, the main difference between the samples was burning time after the pyrolysis height reached the top. Difference in radiation absorption in the visual range did not seem to affect the flame spread noticeably.

For masonite (Figure 4) it was extremely difficult to measure pyrolysis height due to the original color of masonite which did not change significantly with flame spread. Therefore, data for pyrolysis height are omitted. The flame spread rate was not as fast as PMMA. The spread stopped before it reached the top (1.2 m). Data for cardboard (Figure 5) clearly show that the flame spread ceased after 300 s. Cardboard data were obtained in the previous year, but those results are presented here for

completeness. In both cases, the pyrolysis front caught up with the flame height so that the forward heat flux at that point was not sufficient to maintain the flame spread.

Flame spread for the polyurethane foam (Figure 6) was so fast that it was practically impossible to accurately measure the pyrolysis front, so data for pyrolysis front were dropped. Entire spreading occurred within 15 s after the burner was put in place.

Figure 7 shows the results for solid white pine wood board. The flame height peaked at 120 s and steadily decreased. During that time the pyrolysis front moved to 32 cm but it failed to progress further. Two other burner strengths were used to test the influence of burner strength on maximum pyrolysis height. The results are shown in Table 1 below. Average flame height during the flame spread for these three cases are shown in Figure 8. The flame height growth rates at the beginning of the test were about the same but there were differences in the maximum flame heights as well as the time needed to reach the maximum height.

Table 1. Maximum Pyrolysis Height for White Pine as a Function of Burner Strength.

Burner Strength (kW/m)	Burner Flame Height (m)	Maximum Pyrolysis Height (m)
18.0	.29	.32
9.6	.20	.27
6.2	.15	.23

The only textile material tested at Penn State was red velour. The time history of flame height can be seen in Figure 9. It grew quickly and leveled off at about 0.4 m. There was no significant flame spread beyond that point.

Data for another textile material, velvet polyester, and for particle board are also presented and compared with predictions in a later section, which were obtained previously at NIST.

Heat Feedback Results:

Total heat fluxes at five different heights were recorded by Gardon-type heat flux gages at five second intervals. The results for various materials are shown in Figures 10 through 16. In these figures, there are values well above 30 kW/m^2, but a careful interpretation is needed for accurate assessment of these values. Once the pyrolysis height reaches a heat flux gage, the output of the gage becomes erroneous due to the possibility of melted fuel sticking to gage surfaces. Figure 10 shows results for black PMMA. According to Figure 2, gage number 1 provided good data until 70 s and gage number 2 until 140 s. Since pyrolysis height data were available only up to 0.44 m, it was unwise to extrapolate beyond that point. Clear PMMA data are shown in Figure 11 and in this case the PMMA plate warped during the spread causing separation between gage surface and PMMA surface. Therefore, the data for heat flux in this case were not very useful. Figure 13 shows a good example of how the flame spreads along the surface of vertical wall. The output of gage number 1, situated at the height of 0.1 m, first increased, then leveled off at 30 kW/m^2 around 50 s. Gage number 2 peaked at around 150 s, which is the approximate time when the pyrolysis height reached gage number 2 (0.28 m) as seen in Figure 5. Gage number 3 followed a similar pattern. It peaked at around 300 s, which is the approximate time at which the pyrolysis height reached the location of gage number 3, i. e., 0.5 m. Figures 14,15 and 16 can be also explained in the same manner.

Data for total heat flux vs. time at five different heights were normalized by flame heights at various time steps and are shown in Figure 17 for black PMMA. Similar data for masonite, cardboard, polyurethane

foam, white pine, and red velour are shown in Figure 18 through 22. As stated earlier, we were interested in the forward heat flux data (heat feedback from flames to the unburned fuel), therefore, only the data above the pyrolysis height are included in these figures. Since the flame spread was too fast for polyurethane foam to determine when the pyrolysis front passed a certain gage height, Figure 20 includes all data points available. A major outcome of these results is the correlation for forward heat flux, which is described in Appendix II.

Upward Flame Spread Model

In the last annual report, a model for upward flame spread was described which made use of an integral equation for calculating the surface temperature history of the fuel wall using a specific heat feedback distribution. In the new development made in the past year, some of the restrictions were removed and the equations were written in two-dimensional partial differential form (instead of one-dimensional integral form) which are more amenable to numerical solution. Also, the model for heat feedback has been refined and some of the boundary and initial conditions have been modified to reflect a more accurate situation. Thus, the current model is a significant improvement over the previous version.

The overall objective here is to present a *complete prediction procedure* for upward flame spread on practical materials which uses a fundamentals-based mathematical model, along with the available properties *and* appropriately defined additional properties, termed here, "fire properties". As described later, the additional properties will allow one to take into account the nonideal behavior of practical materials (or, the "material signature") as they burn in vertical wall-type configuration, while keeping the computations manageable and accuracy acceptable.

General Description:

A physical model for upward flame spread is depicted in Figure 23. A vertical combustible wall with infinite width is ignited at the bottom. When making computations for comparison with data, the sample was assumed

to be of 1.2 m height in order to simulate the geometry in the experimental setup. A natural gas line burner with a typical strength of 18 kW/m is placed at the bottom of the vertical wall sample. Because of the heat flux provided by the flames of the burner, the surface temperature of the bottom section of the wall rises until it reaches a certain characteristic temperature (T_{ig}) at which time the material starts pyrolyzing significantly. Then, flames from the burning of pyrolyzed fuel continuously cover the solid fuel above the pyrolysis front (x_p), which is heated by the energy feedback ($\dot{q}''_w$) from the flames. When the unburnt fuel heats up to T_{ig}, it starts pyrolyzing, the flames grow taller, and thus, the process of upward flame spread continues. The important parameters contributing to the upward flame spread, therefore, are the heat feedback from flames to unburnt wall surface, $\dot{q}''_w(x,t)$, mass loss rate of the wall on the pyrolyzing surface, $\dot{m}''(t)$, the flame tip height, $x_f(t)$, and other physical and chemical material properties such as ignition temperature (T_{ig}), heat of combustion (h_c), thermal conductivity (k), density (ρ), and heat capacity (c_p).

In the present study, the mathematical model has been developed to accept certain measurable fire properties obtained from small scale experiments in order to predict the upward propagation of fire on a vertical wall made of practical materials having a finite thickness, which are briefly described below.

The unique way in which we account for the burning of practical materials of finite thickness is through the definition of a fire property function of the material under consideration, $\dot{m}''(t)$, which is the local transient mass loss rate during the turbulent combustion of a vertical flat sample burning in a configuration similar to that during upward flame spread. This property includes (a) a finite burning period for the given wall material under consideration reflecting the finite thickness of the material and, (b) the time history of the mass loss rate as the material burns, reflecting such characteristics as charring, laminated or composite structure, and unsteady heat loss in the interior of the sample. When measuring $\dot{m}''(t)$, a sample of the material is subjected to similar conditions as those of the yet-unburnt material just above the pyrolysis front. In a typical upward flame spread situation in a room fire, flame height scales of

several centimeters to just over two meters are common. In that case, flames are turbulent and the heat feedback from flames to the wall is around 25 +/- 5 kW/m^2. These conditions are simulated in the measurement of $\dot{m}''(t)$. While this is not claimed to be the perfect representation of the burning material during upward flame spread, it is reasonably accurate and convenient for describing and assessing the behavior of the material and for using it in a mathematical model. Other approaches to estimate or predict $\dot{m}''(t)$ have involved too many assumptions and simplifications (such as a constant $\dot{m}''(t)$ throughout), or made use of too many properties for the material which are generally unavailable, and even if some of them are, there is often too much uncertainty in those property values. A complete description on the definition, measurement, and evaluation of this property, $\dot{m}''(t)$, is given in Appendix III.

The second fire property we have defined for the model is the characteristic forward heat feedback, $\dot{q}''_{wo}$. It is the total heat flux from flames to a location just above the pyrolysis front. If a material burns with flames having a large amount of soot, the flame heat feedback to the wall is enhanced due to radiation. This effect is appropriately taken into account by the characteristic forward heat feedback, $\dot{q}''_{wo}$. It is defined later in the development of the mathematical model. The measurement and justification of $\dot{q}''_{wo}$ is given in detail in Appendix II.

Governing Equations:

Since the flame spread rate is directly related to the time history of the pyrolysis height which is defined as the height at which the surface temperature reaches ignition temperature, we need to calculate the surface temperature to get the pyrolysis height. It is assumed that the ignition temperature does not vary with location and the material is inert during the heating process. The surface temperature as well as the inside temperature of the two-dimensional vertical slab, initially at the temperature of T_o, are obtained by solving transient two dimensional heat conduction equation,

$$\frac{\partial T}{\partial t} = \alpha\left(\frac{\partial^2 T}{\partial x^2} + \frac{\partial^2 T}{\partial y^2}\right), \tag{2}$$

with the transient boundary conditions,

$T(x,y,0) = T_o$,

$T(x,0,t) = T_{ig}$ for $x < x_p$,

$$-k\frac{\partial T}{\partial y}\bigg|_{y=0} = \dot{q}''_w(x,t) \quad , \quad -k\frac{\partial T}{\partial y}\bigg|_{y=D} = h\,(T - T_o) \quad \text{for } x > x_p,$$

$$-k\frac{\partial T}{\partial x}\bigg|_{x=0} = 0 \quad , \quad -k\frac{\partial T}{\partial x}\bigg|_{x=H} = 0\,, \tag{3}$$

where y=0 to D and x=0 to H represents the domain for calculations. The unstaedy, height-dependent forward heat flux $\dot{q}''_w(x,t)$ is obtained from curve-fitting experimental data and it can be written in the form,

$$\dot{q}''_w(x,t) = \dot{q}''_{wo}\; g\,\{\, x_b(t), x_p(t), x_f(t), x \,\} \tag{4}$$

where $\dot{q}''_{wo}$ is treated as a fire property of the wall material and g is a generalized function of burnout edge (x_b), pyrolysis height (x_p), and flame tip height (x_f). The procedure for obtaining $\dot{q}''_{wo}$ and g is described in Appendix II.

The flame tip height is obtained from an available correlation,

$$x_f(t) - x_b(t) = K\left[\dot{Q}'(t) + h_c \int_{x_b(t)}^{x_p(t)} \dot{m}'' \, dx\right]^n \tag{5}$$

where $\dot{Q}'$ (kW/m) is the igniter strength function . It is given by,

$$\dot{Q}' = \dot{Q}_o' \left(\frac{2x_{fo} - x_b}{2x_{fo}}\right)^2.$$

Here, h_c is the heat of combustion of the fuel, K and n are experimentally obtained constants, $\dot{Q}_0'$ is the initial igniter strength, and $\dot{m}''$ and x_b are described as,

$$\begin{aligned} \dot{m}''(\lambda) &= a_4\lambda^4 + a_3\lambda^3 + a_2\lambda^2 + a_1\lambda + a_0 \;\; ; \text{ if } \lambda < \lambda_b \\ \dot{m}''(\lambda) &= 0 \;\; ; \text{ if } \lambda > \lambda_b \end{aligned} \tag{6}$$

and,

$$x_b(t) = x_p(t - \lambda_b) \tag{7}$$

where λ is a local time which is the time after that local point reaches the ignition temperature and λ_b is the burnout time which is the time period from the instant of ignition to the end of pyrolysis at a given location. As mentioned earlier, the local mass loss rate $\dot{m}''(\lambda)$ is assumed to be a material fire property and independent of the location. Measurement of mass loss rate and a description of the apparatus were described briefly in the last annual report. Appendix III gives a description and results of mass loss rate experiments for several materials used here.

It should be noted that the quantity in brackets in equation (5) is the **rate of heat release (RHR)** per unit width of the wall as a function of time. RHR, and its integral with time, the total heat release, are important quantities in fire hazard studies, especially for consideration of flashover point, time to initiate smoke alarm, and smoke and fire spread in a

multiroom structure. However, in this report we will not pursue discussion on RHR because the focus is on upward flame spread on vertical wall.

Numerical Solution:

The above set of equations is solved with a numerical procedure that involves finite difference method. Because of stiff temperature gradients close to the surface, grid spacing has to be dense near the surface. If uniform spaced grid pattern is used, 1000 nodes in y-direction would be required to have desired accuracy. This problem is solved by using a nonuniformly spaced grid which packs many grid points near the heated surface, and then allows gradual increase in the spacing between grid points. Equations for the grid are,

$$\Delta x = H/(ni-1)$$
$$x_i = \Delta x\,(i-1) \tag{8}$$
$$y_j = D\,\frac{(\beta+1)-(\beta-1)\left\{[(\beta+1)/(\beta-1)]^{1-\frac{j-1}{nj-1}}\right\}}{[(\beta+1)/(\beta-1)]^{1-\frac{j-1}{nj-1}}+1}$$

and the pattern is shown in Figure 24.

Effect of the size of nodes in x-direction on numerical results is shown in Figure 25. The CPU (central processing unit) time for 2 cm size was 48 minutes, for 1 cm was 2 hours, and for 1 mm was 20 hours on a desktop Vax Station 2000. Considering these results, we have decided to use a node spacing of 1 cm in future calculations.

The Prediction Procedure:

The procedure used for predicting the upward flame spread rate (and the transient rate of heat release, if needed) on a vertical wall of a given material or a combination of materials (for example, a wood panel, or a carpet mounted on an inert dry wall material, an aircraft panel, etc.) is as follows. First, the physical properties of the material of T_{ig}, h_c, k, ρ, and c_p are needed. These properties may be either found in the literature or from a standard small scale fire test apparatus such as LIFT (developed at NIST).

Two other properties, $\dot{m}''(t)$ and $\dot{q}''_{wo}$ are found from small scale experimental setups described in Appendices II and III. An average heat transfer coefficient for heat loss from the back side of the wall is selected (which may be based on natural convection or forced convection, depending on the situation, however, results are not very sensitive to this value). The above numerical procedure is then employed to predict the spread of flame tip height and the pyrolysis height as a function of time.

Discussion:

Comparison of predictions and data for the flame height and pyrolysis height for black PMMA, masonite, and cardboard are shown in Figures 26, 27, 28, respectively. The bars in Figure 27 for masonite indicate the range of x_f due to flame fluctuations. The flame height is constant up to approximately 60 s because the material has not yet started pyrolyzing and the flames are entirely from the gas burner. After 60 s, the sample starts pyrolyzing and thus the flame height and pyrolysis height grows. The trends and magnitudes of the flame height, and therefore the upward flame spread, are clearly well-predicted by the model for masonite as well as for the other two materials. Figure 26 shows **accelerating** nature of flame spread for PMMA. It predicts the flame height very accurately, but it overpredicts the pyrolysis height. In Figure 28 the model correctly predicts the end of flame spread because the pyrolysis height becomes equal to the flame height so that forward heat flux is not enough to sustain flame spread. This clearly demonstrates the model's ability to predict the **end of flame spread.**

Figures 29 shows comparison of data and predictions for 0.0127 m thick white pine board. In this case the transient mass loss rate ($\dot{m}''(t)$) measurements could not be made accurately in our existing apparatus without modifying it substantially because the combustible mass, as a fraction of the total weight of the sample, was very small. The correction in mass loss rate data (see Appendix III for details) was in the same order of magnitude as mass loss rate. Therefore, an alternative, but approximate approach was used to estimate $\dot{m}''(t)$. The $\dot{m}''(t)$ was assumed to be *constant*, not transient, which was determined from the total combustible mass and burnout time period. The following value was used :

$$\dot{m}''(t) = 0.005598 \text{ kg/m}^2\text{s}$$

The predictions for white pine do not agree quite well with the data, however, following two points should noted: (i) the order of magnitude of x_f is similar to that predicted and (ii) the use of constant $\dot{m}''(t)$ can explain the difference in the trends . Most woods give off a large amount of volatiles in the initial stage of combustion, but later, the burning rate tapers off slowly. A constant average value of $\dot{m}''(t)$ is thus expected to underpredict the data initially and then overpredict it, as seen in Figure 29.

Figure 30 shows data and predictions for a textile material red velour. Here too the $\dot{m}''(t)$ could not be determined in the existing apparatus because of the small mass of the sample, and also no other property data were available. Therefore, property data for a similar other fabric, velvet polyester, obtained previously at NIST, were used. The flame advanced very little beyond the flame height of the igniter before the end of flame spread. In view of this fact, and considering the approximation in property data, the predictions compare reasonably well with data in Figure 30.

Figures 31 and 32 show data and predictions for the textile material, velvet polyester, and 0.0127 m thick particle board. These two materials were not tested at Penn State; the data were obtained from tests conducted at NIST in 1988. The comparison of data with predictions are seen to be reasonably good for velvet polyester but data are underpredicted for particle board. The particle data are often strongly influenced by humidity, and since we are not exactly sure of the circumstances for these experiments, this case is under further consideration.

Some improvements can be made to the model and the overall prediction procedure presented here, such as the inclusion of a nonconstant ignition temperature (like in charring fuels), indepth radiation absorption of flame radiation at the pyrolyzing surface, effect of variation of the fire properties $\dot{q}''_{wo}$ and $\dot{m}''(t)$ with the height (although it is expected to be minor for a typical room size fire), etc. However, these effects are of "second order", and the current model appears to be accurate and quite adequate for engineering studies, especially considering the property data base currently available for practical materials. In contrast, mathematically rigorous

models, which attempt to predict $\dot{m}''(t)$ and $\dot{q}''_{wo}$ will require many more properties as input to the model, which are (i) often not available, and/or (ii) available with very poor accuracy, and/or (iii) fail to appropriately capture the special material characteristics (material "signatures"), in addition to requiring inordinate amount of computer time, making the models effectively impractical. An extension of the proposed study is currently under progress for allowing effect of the surrounding fire conditions (strong external radiation incident on the wall) on upward flame spread.

A special note is warranted for the two newly defined fire properties in this work. These two properties, when examined in conjunction with the forward heat flux shape function *g* (equation 4), are seen to be the key factors in promoting the upward flame spread. They can be viewed as the indicators of the performance of the materials in the configuration of upward flame spread on a vertical. Therefore, the two properties may be used to rank various materials in terms of their flammability in the upward flame spread mode, which is often the most critical mode of fire spread for hazard estimation. Thus, these two properties, or a combination of the two, should be explored to establish a **standard flammability test procedure.**

Summary and Conclusions

This work describes results of a comprehensive study of turbulent upward flame spread on vertical walls made of finite thickness, practical materials. A complete prediction procedure is proposed using a fundamentals-based mathematical model employing appropriately defined fire properties of wall materials, *viz.* the transient mass loss rate under typical turbulent wall fire conditions ($\dot{m}''(t)$) and a characteristic forward heat flux ($\dot{q}''_{wo}$). Procedures for determining these properties are also presented. A numerical procedure is given to solve model equations. Experimental data on flame height, pyrolysis height, and heat feedback from flames to the wall, are presented for several materials currently in practical use. Data and predictions are compared to validate the prediction

procedure and a suggestion is made for establishing a flammability standard for upward flame spread.

The most important feature of this investigation is that the proposed *complete prediction procedure* is useful for *practical* materials under realistic wall fire conditions. The wall material may possess special characteristics (such as early volatilization, charring, composite or laminated structure, etc.) and may burn as a thin material (with unsteady heat loss to the interior due to finite thickness). Thus, the present method can be used in fire hazard prediction studies or in testing wall materials for their flammability characteristics in the upward flame spread configuration.

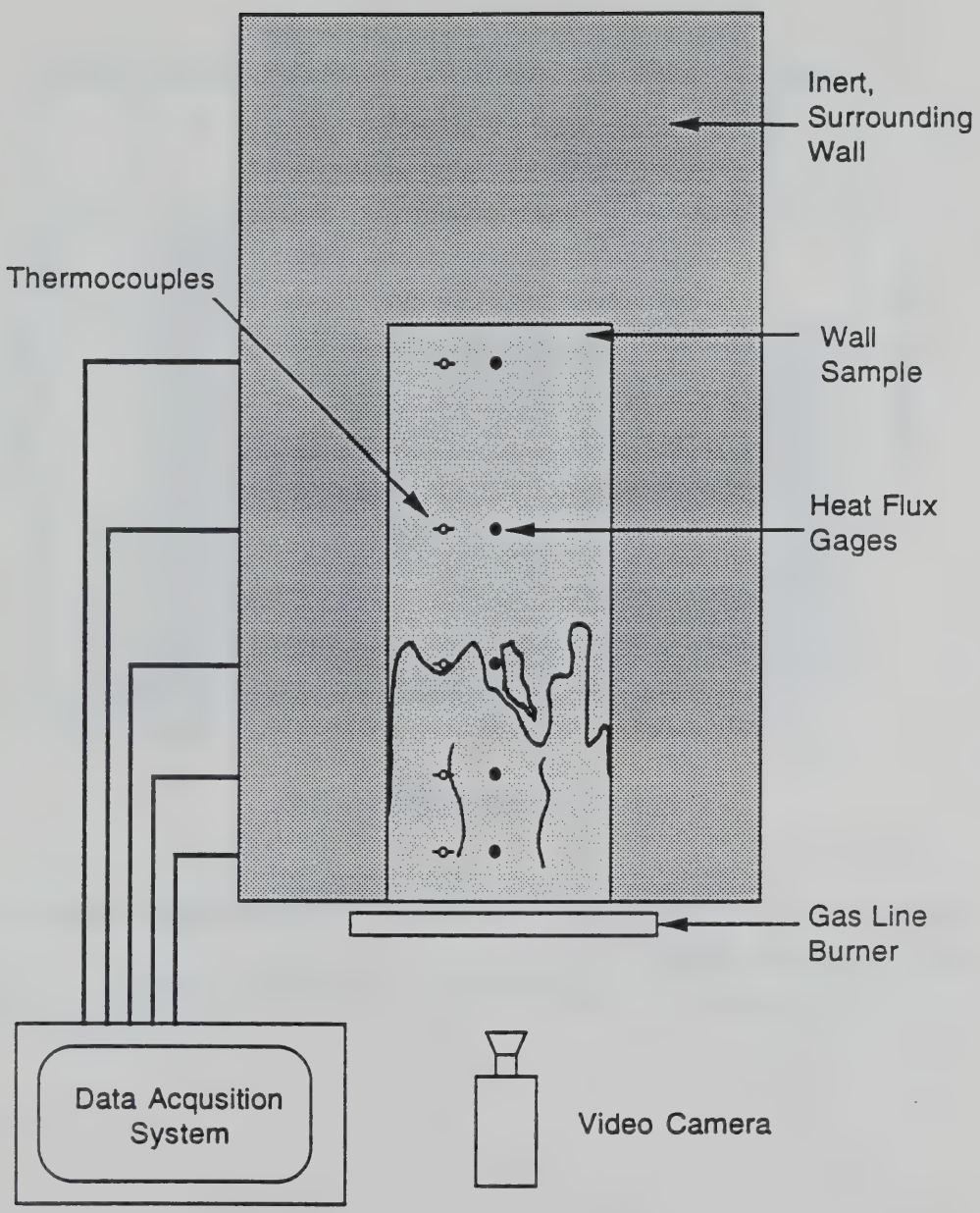

Figure 1a. Schematic of Apparatus for Turbulent Upward Flame Spread Experiments.

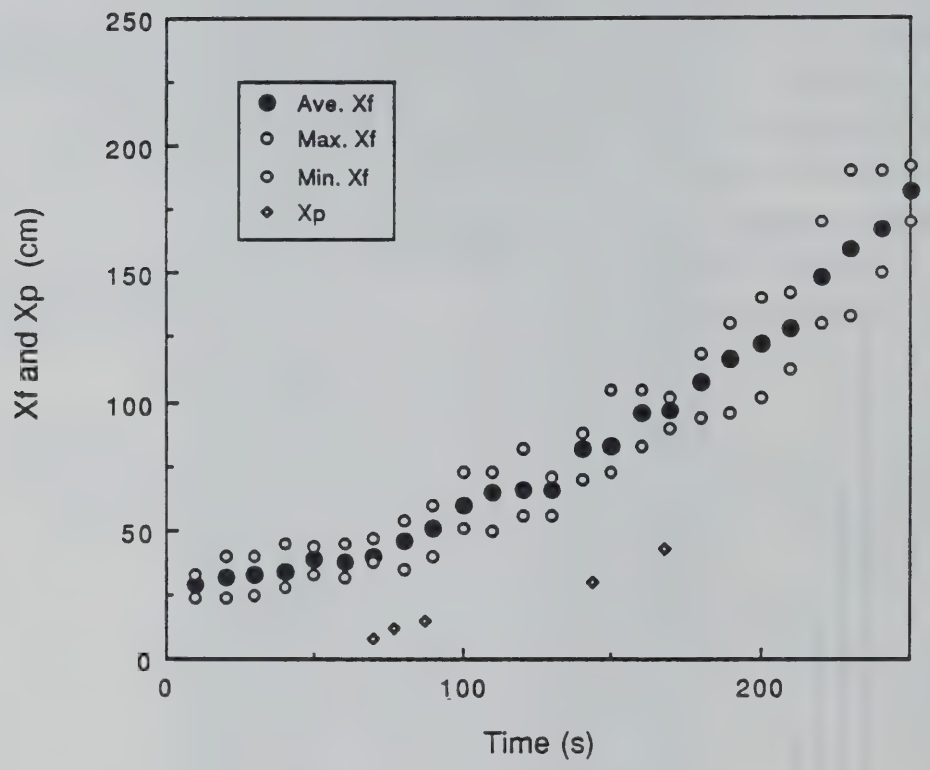

Figure 1b : A sample data set showing flame height, its fluctuations, and pyrolysis height.

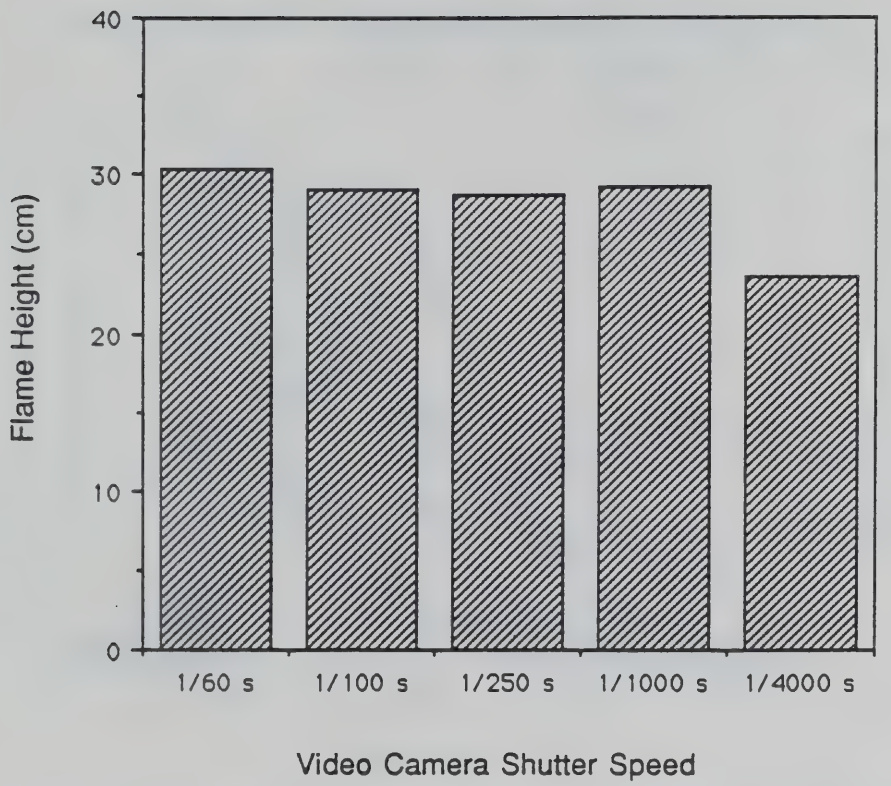

Figure 1c : Influence of camera shutter speed on flame height measurement.

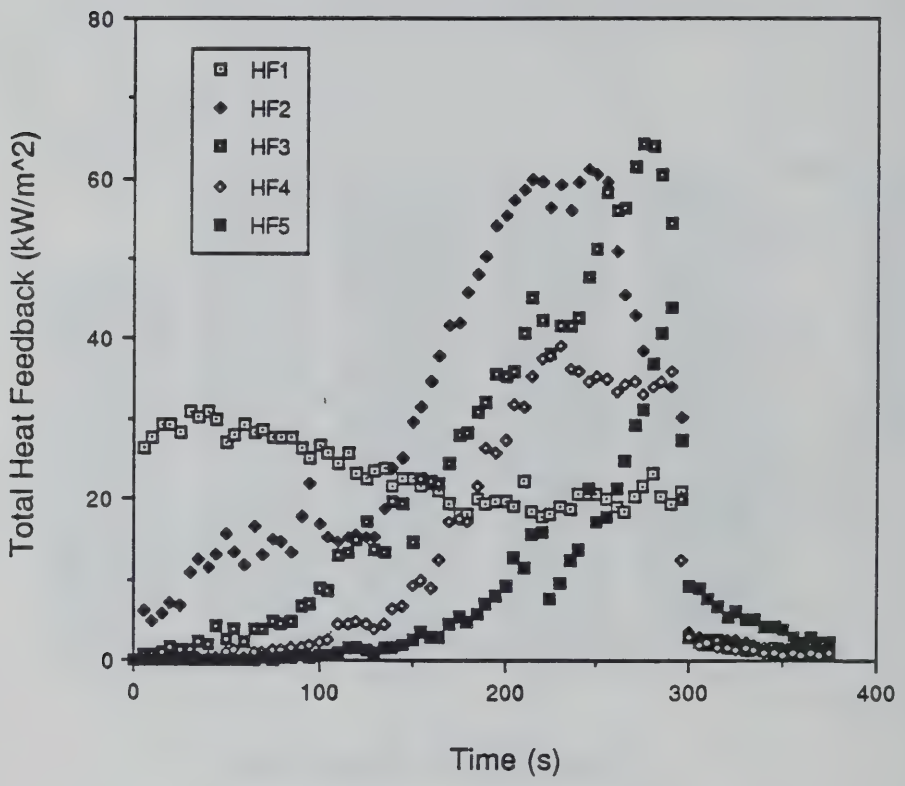

Figure 1d : A sample data set showing the total heat feedback measured by five heat flux gages. As indicated in Fig. 1a, heat flux gage number 1 (HF1) is closest to the igniter near the bottom and HF5 is at the top.

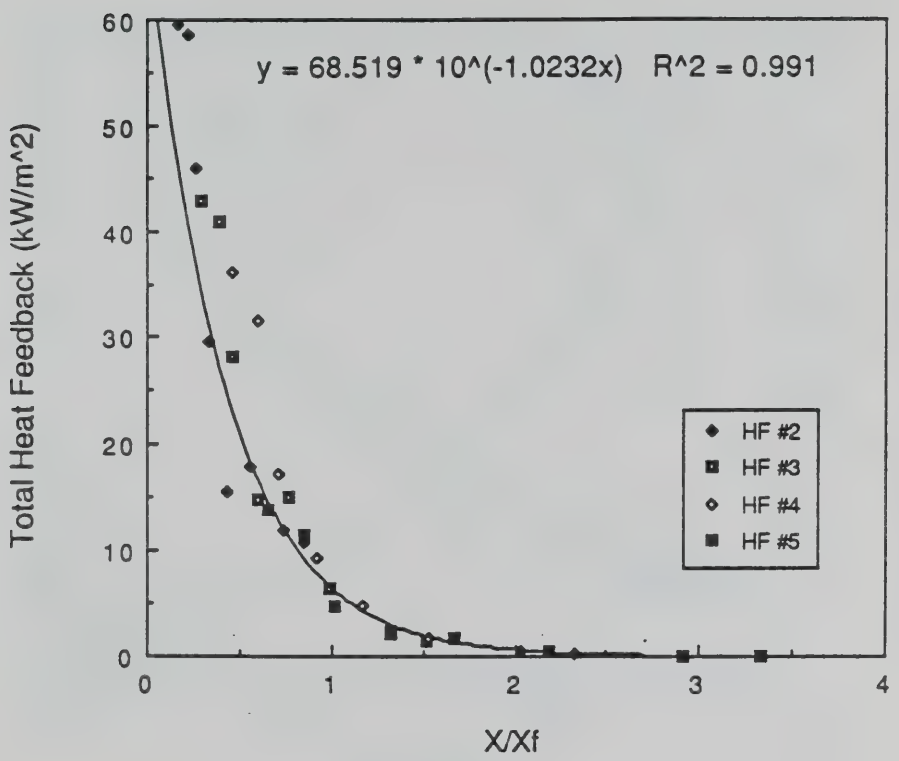

Figure 1e : Total heat flux data of Fig. 1d replotted against height normalized by instantaneous flame height.

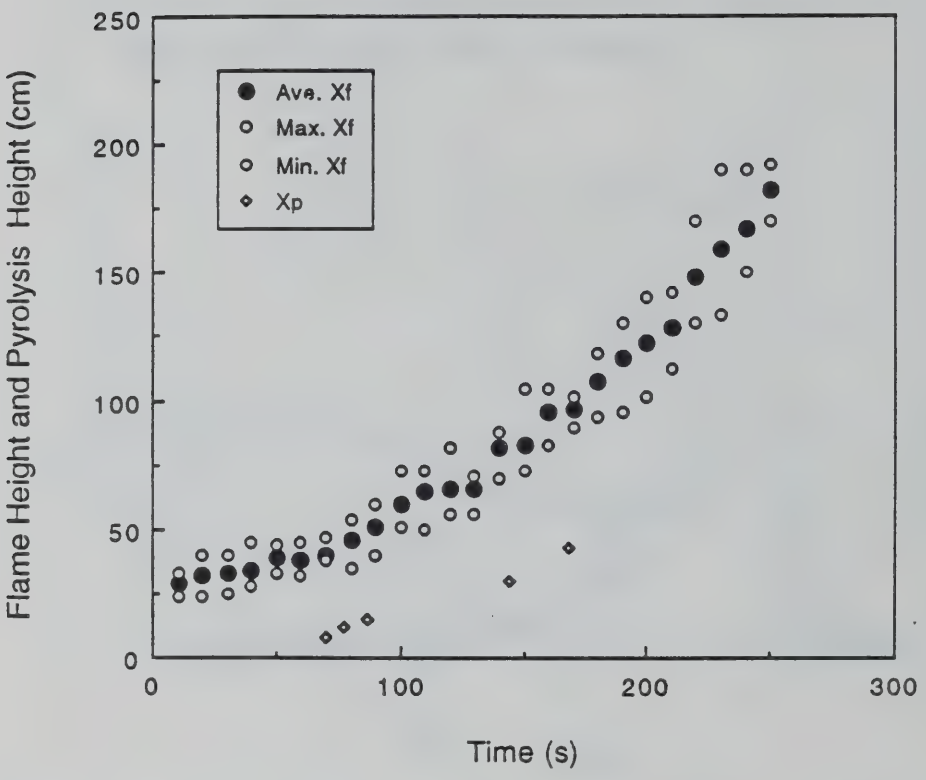

Figure 2. Measured Flame Height and Pyrolysis Height History for 0.003175 m Thick Black PMMA.

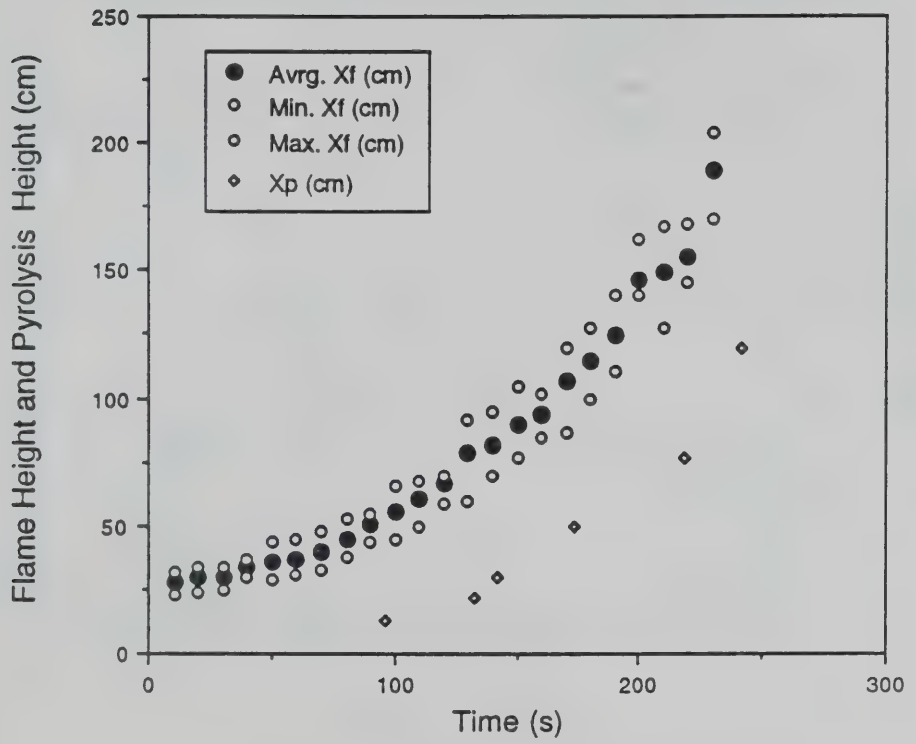

Figure 3. Measured Flame Height and Pyrolysis Height History for 0.001588 m Thick PMMA.

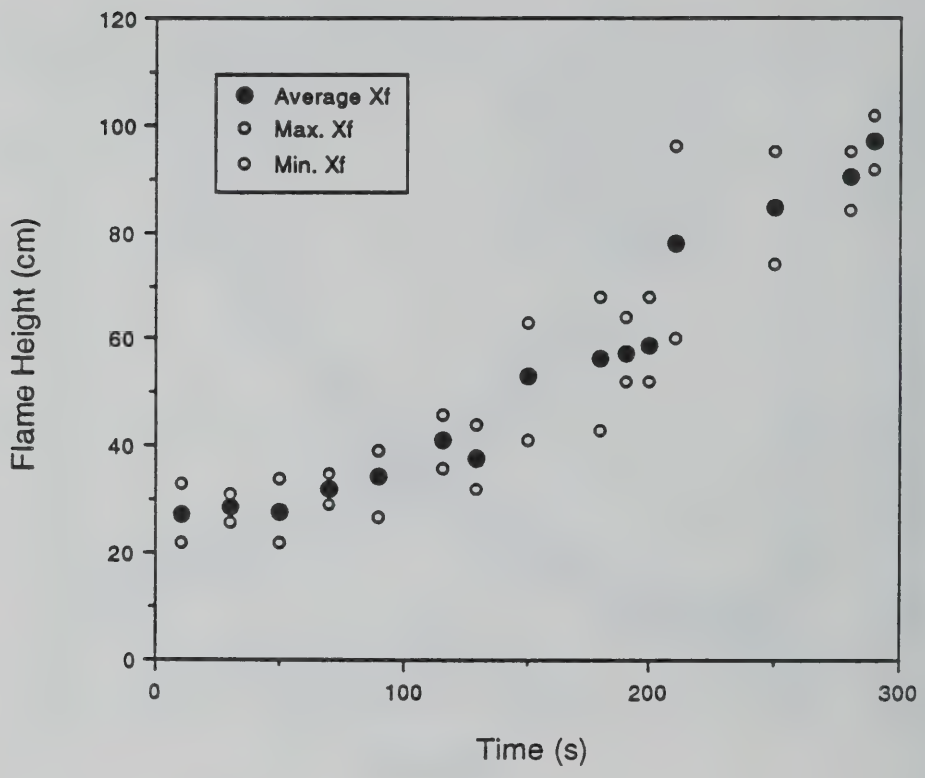

Figure 4. Measured Flame Height History for 0.003175 m Thick Masonite Board.

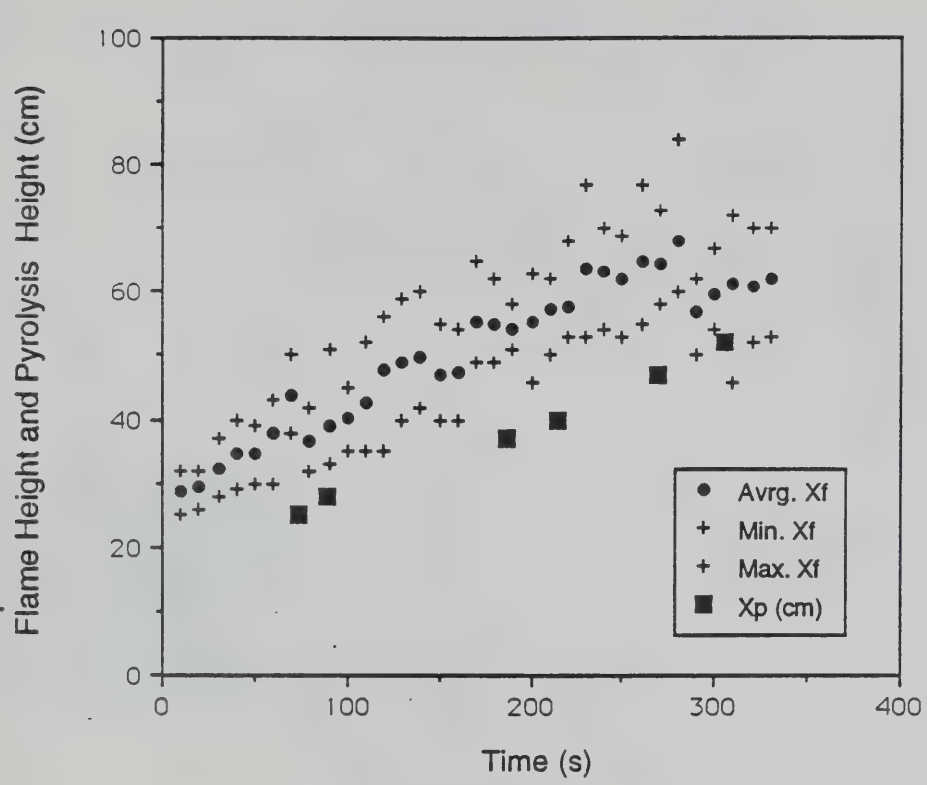

Figure 5. Measured Flame Height and Pyrolysis Height History for 0.005 m Thick Card Board.

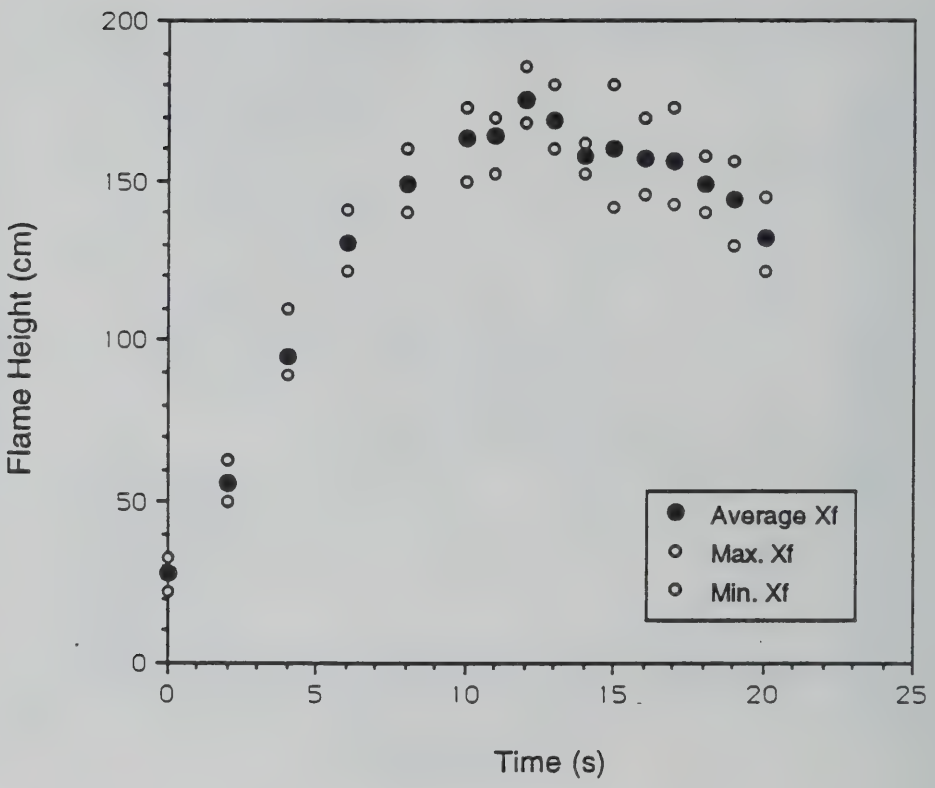

Figure 6. Measured Flame Height History for 0.0127 m Thick Polyurethane Foam.

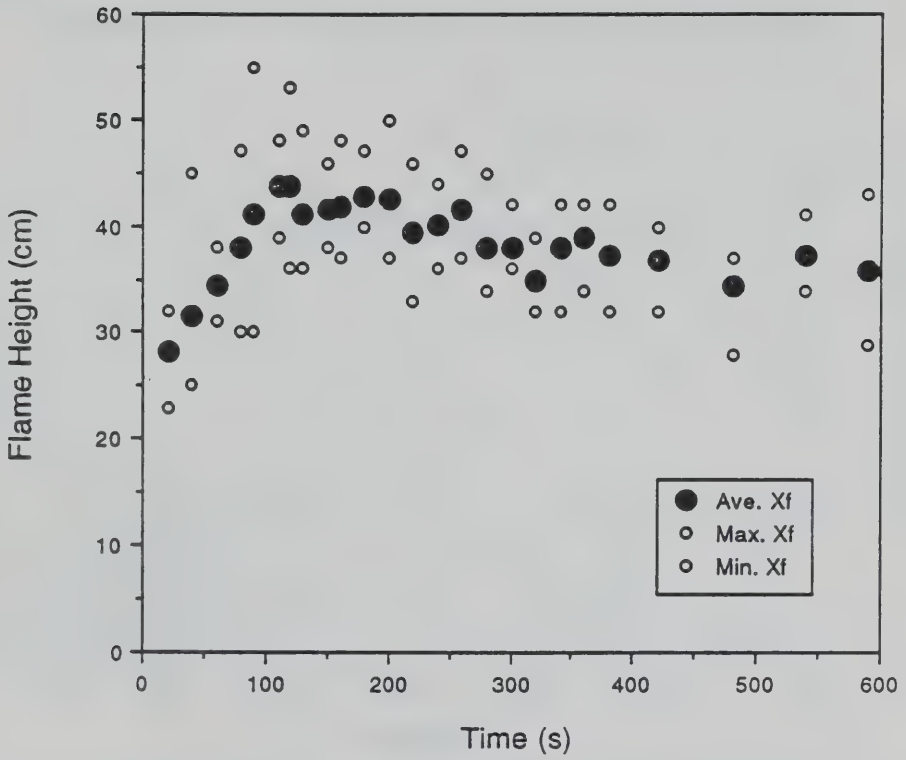

Figure 7. Measured Flame Height History for 0.0127 m Thick White Pine Board.

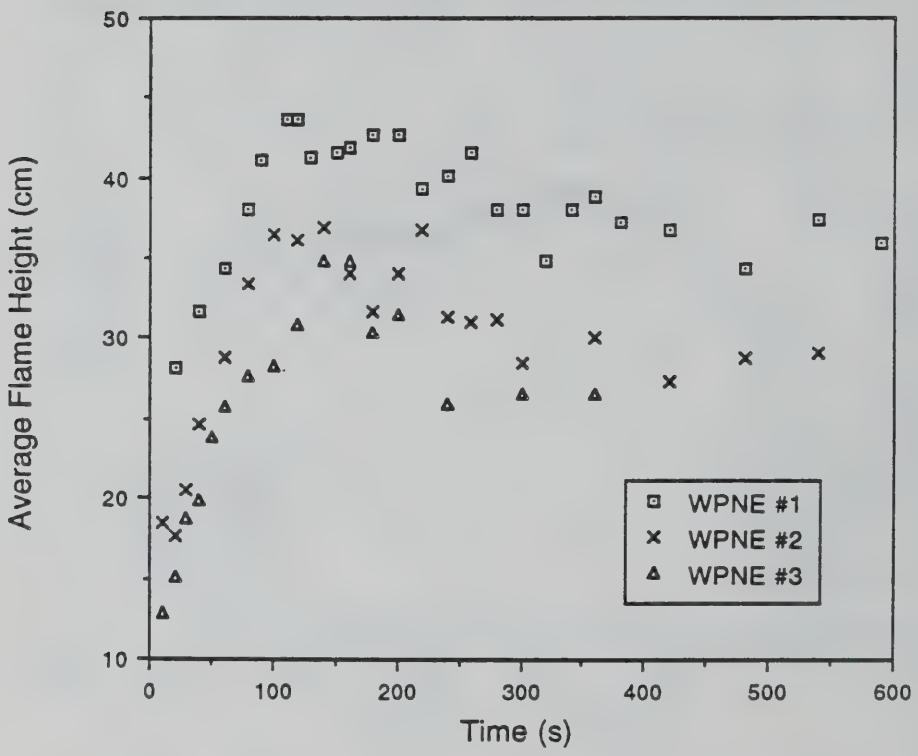

Figure 8. Measured Average Flame Height for 0.0127 m Thick White Pine Board with Various Igniter Strengths: #1, 18 kW/m; #2, 9.6 kW/m; #3, 6.2 kW/m.

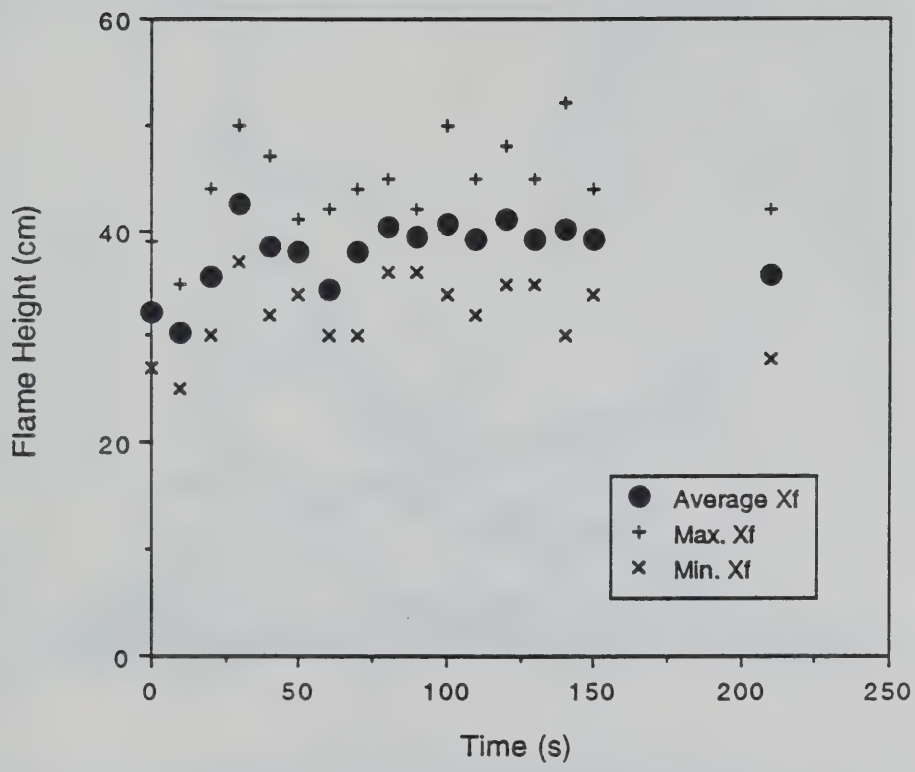

Figure 9. Measured Flame Height History for 0.0012 m Thick Red Velour Fabric.

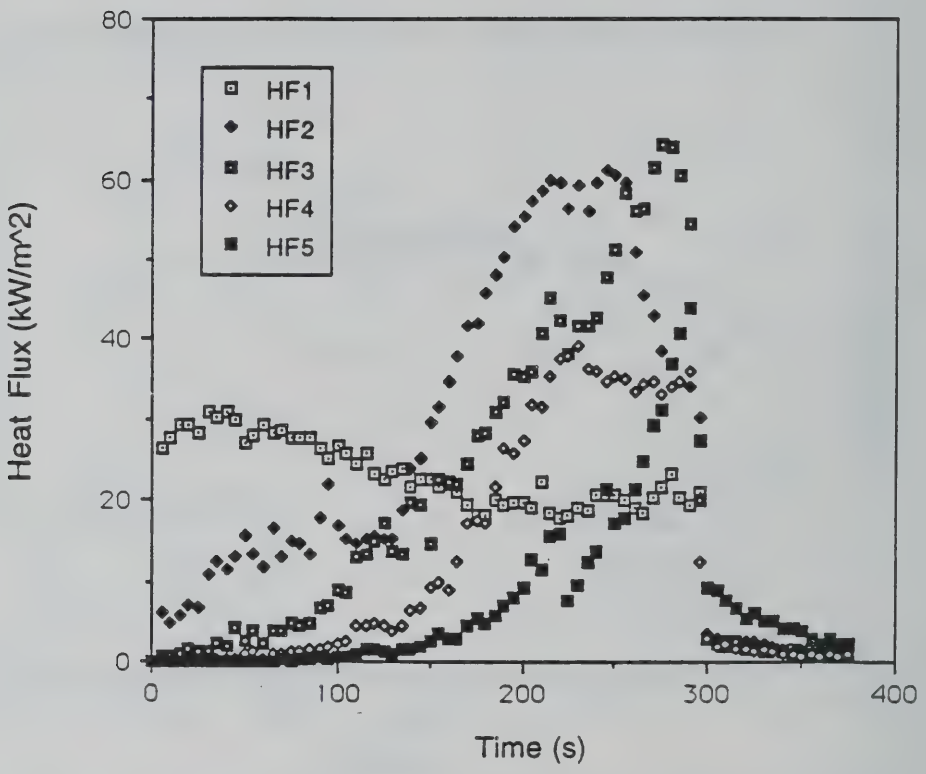

Figure 10. Total Heat Flux History for 0.003175 m Thick Black PMMA at Five Different Heights.

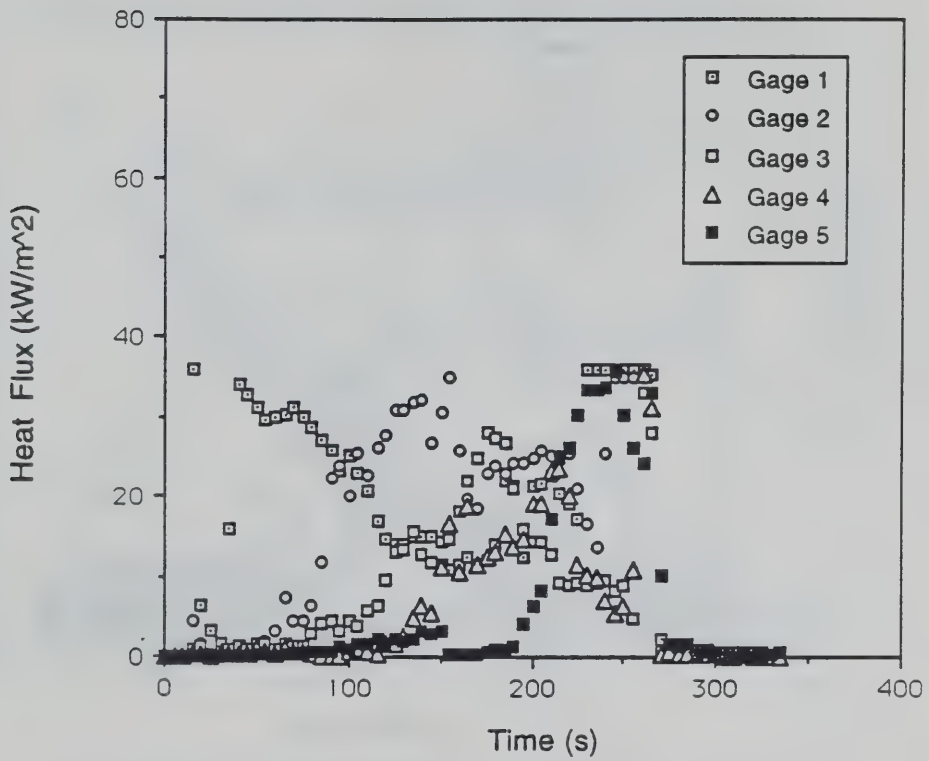

Figure 11. Total Heat Flux History for 0.001588 m Thick PMMA at Five Different Heights.

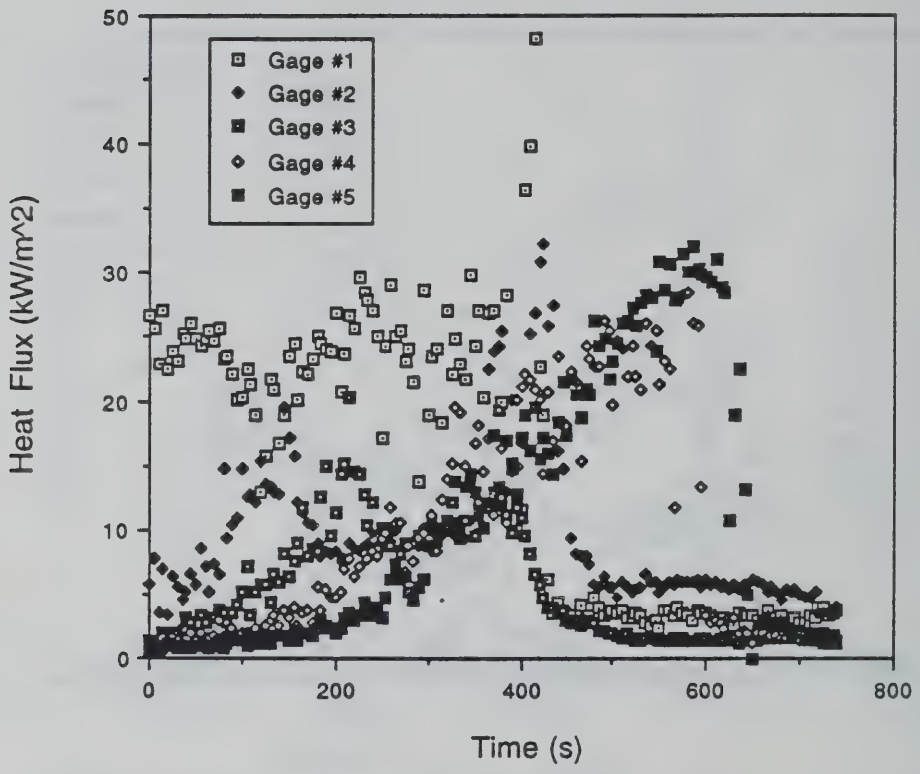

Figure 12. Total Heat Flux History for 0.003175 m Thick Masonite Board at Five Different Heights.

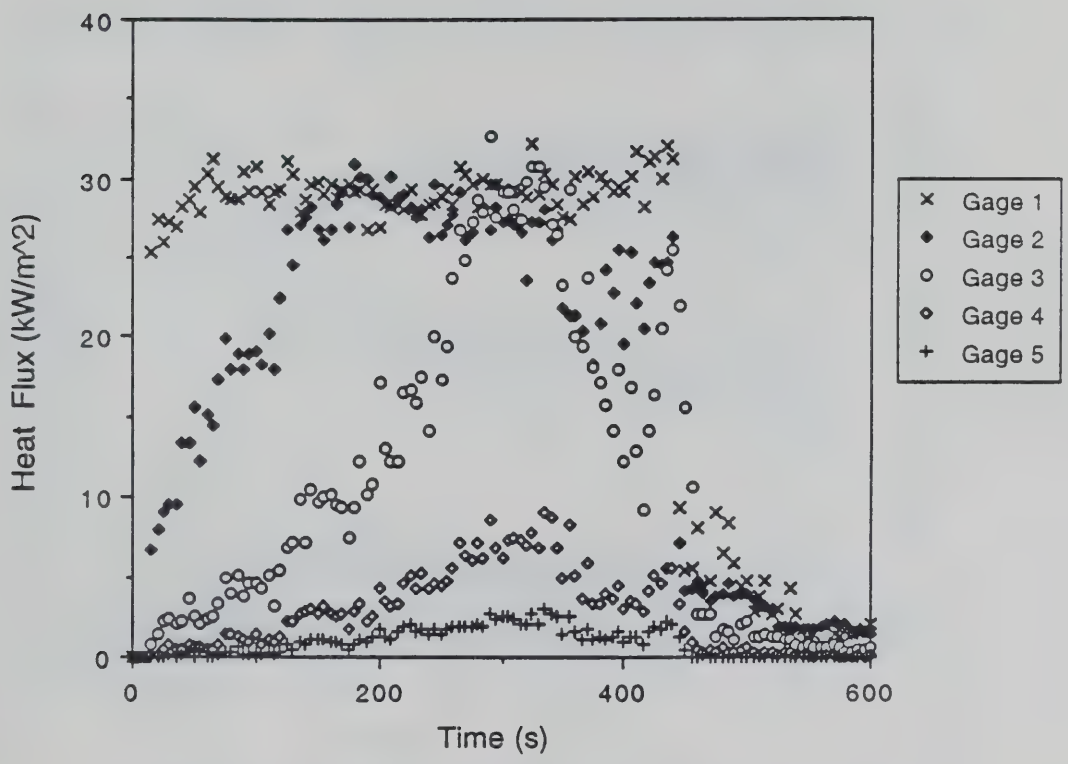

Figure 13. Total Heat Flux History for 0.005 m Thick Card Board at Five Different Heights.

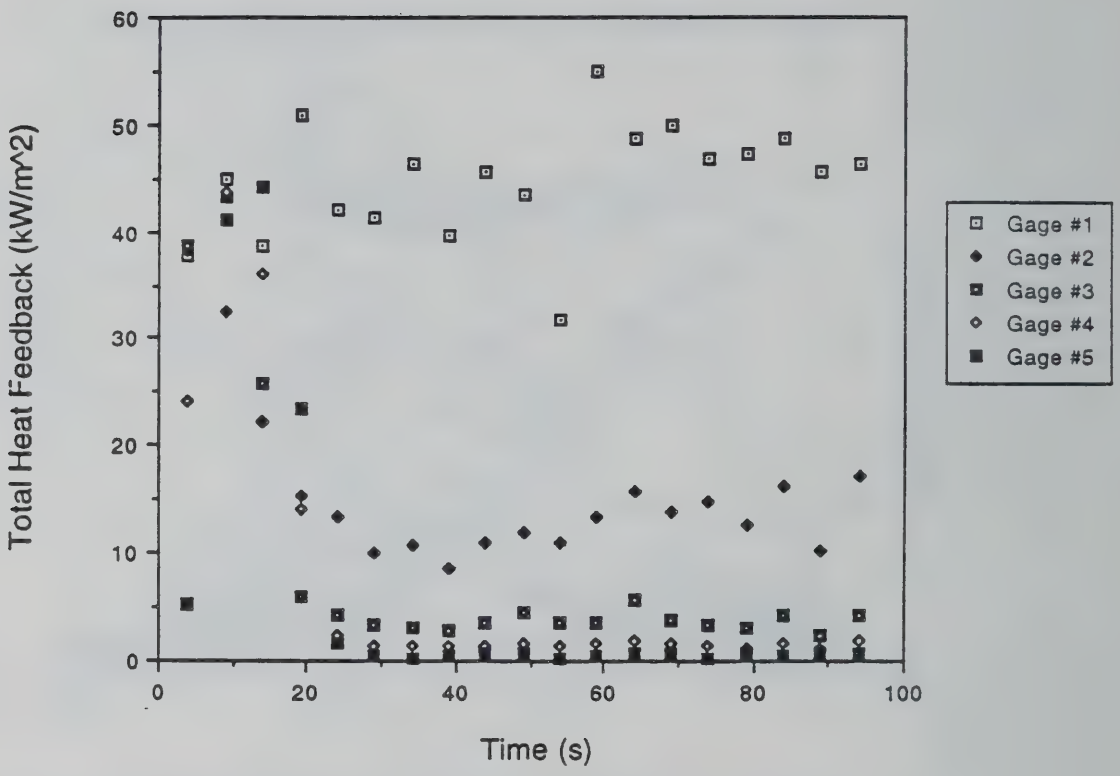

Figure 14. Total Heat Flux History for 0.0127 m Thick Polyurethane Foam at Five Different Heights.

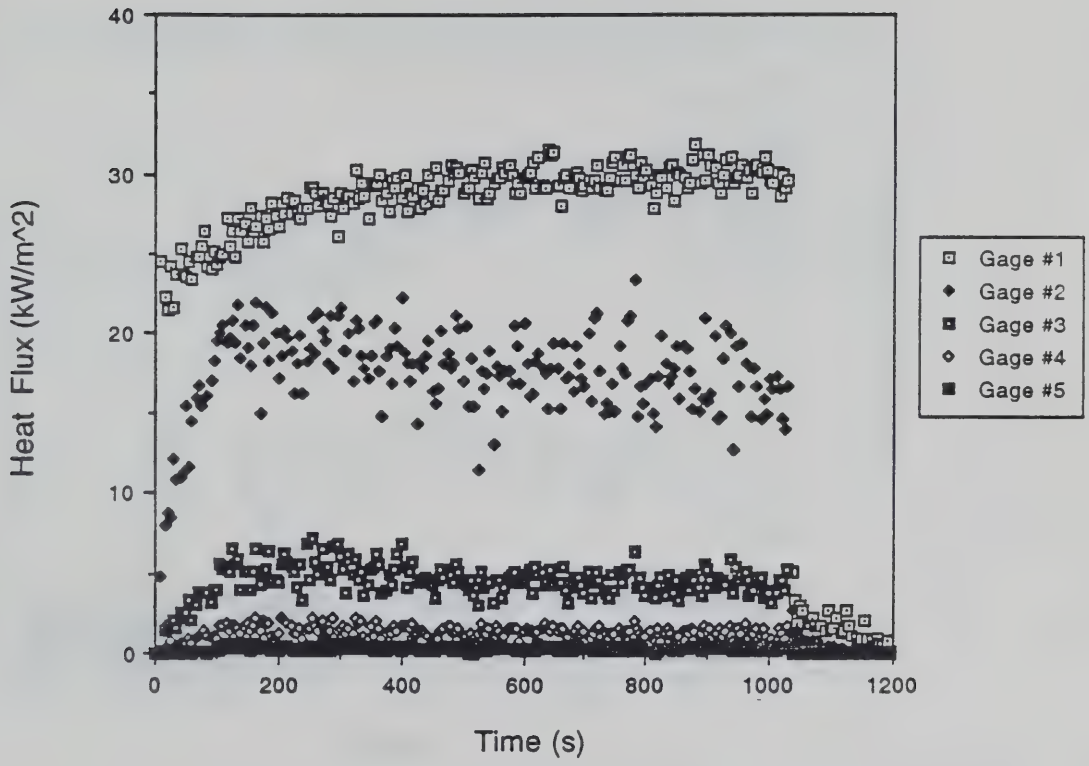

Figure 15. Total Heat Flux History for 0.0127 m Thick White Pine Board at Five Different Heights.

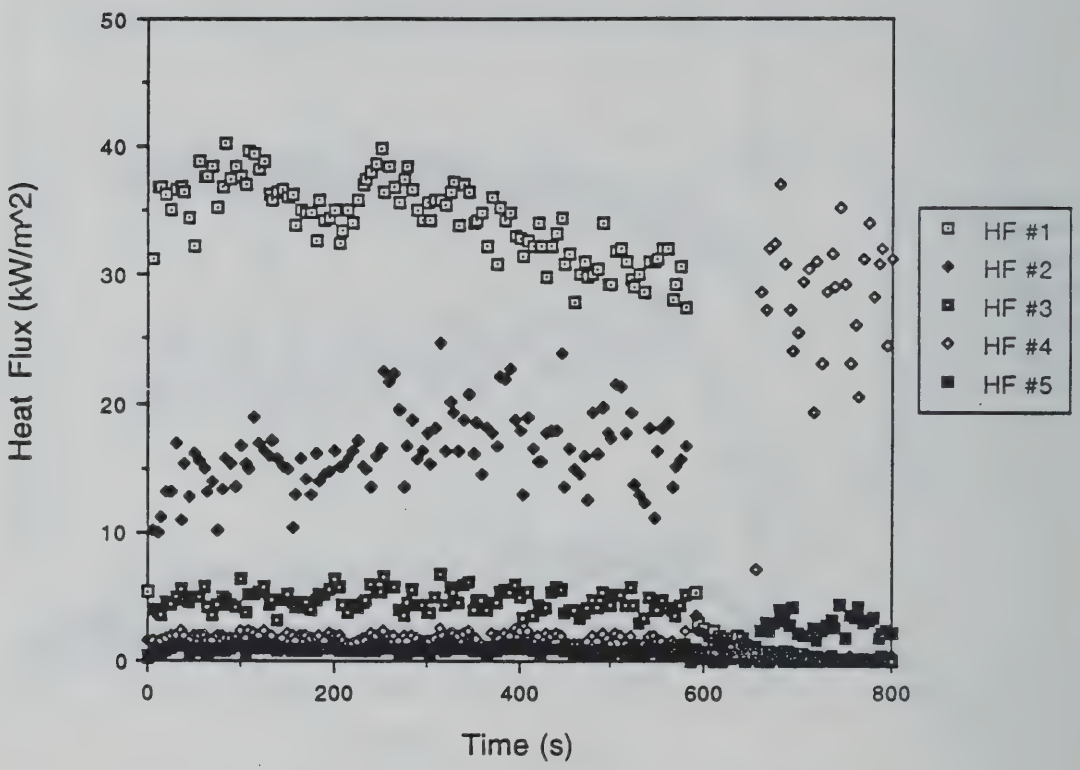

Figure 16. Total Heat Flux History for 0.00127m Thick Red Velour Fabric at Five Different Heights.

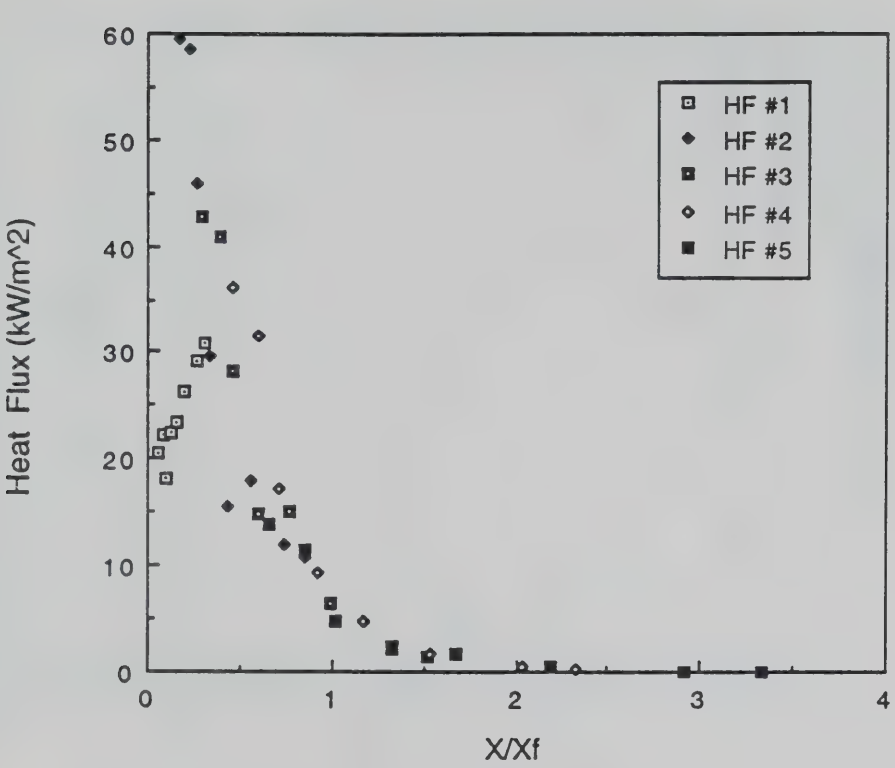

Figure 17. Total Heat Flux vs. Normalized Height for 0.003175 m Thick Black PMMA Board.

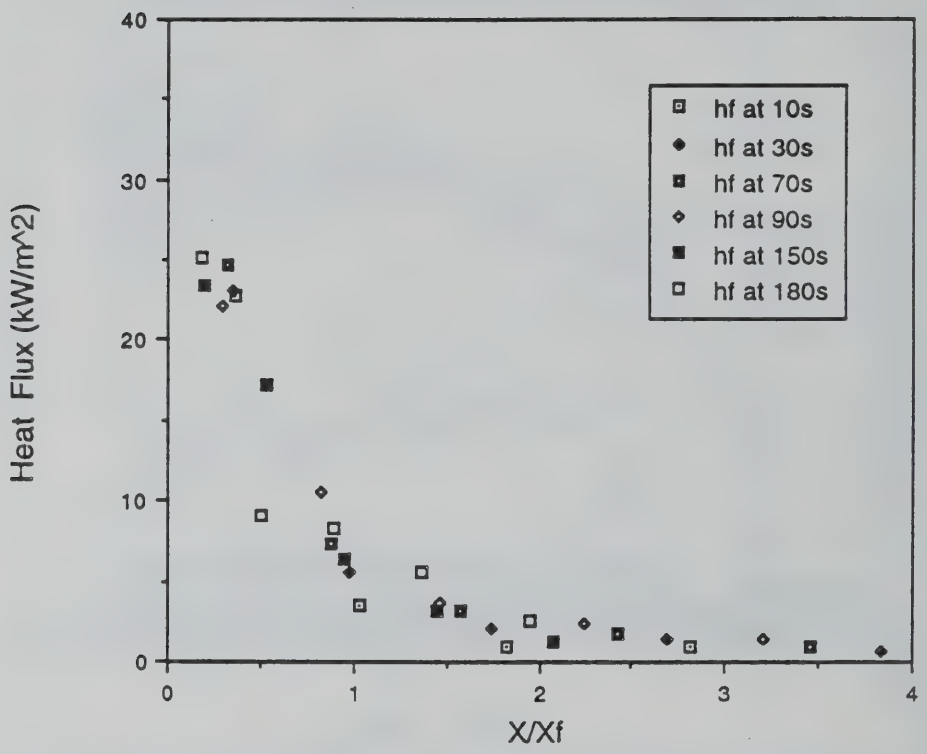

Figure 18. Total Heat Flux vs. Normalized Height for 0.003175 m Thick Masonite Board.

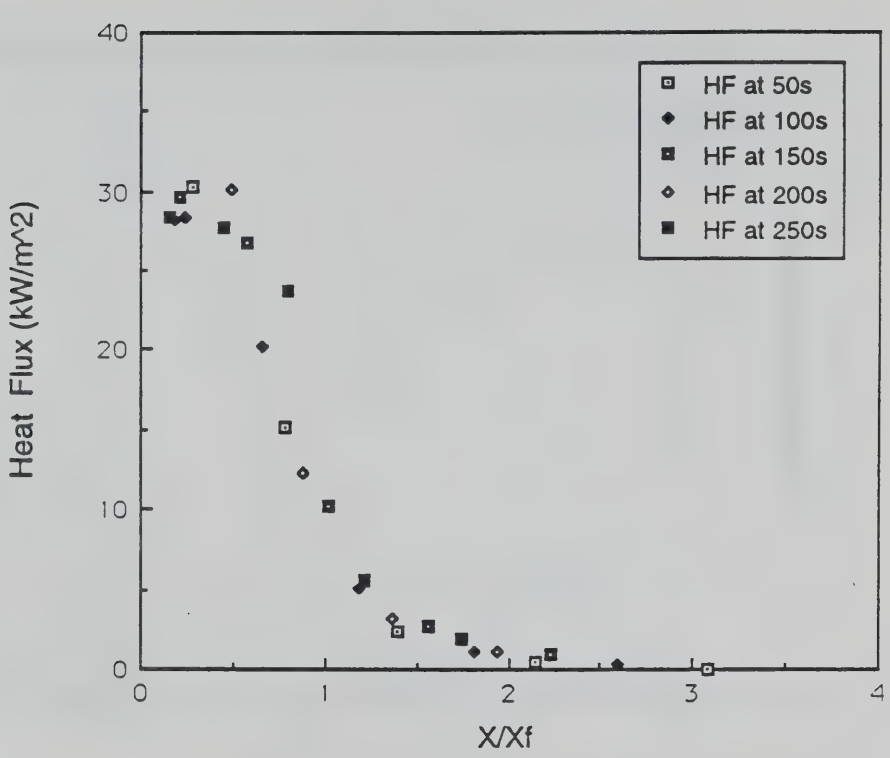

Figure 19. Total Heat Flux vs. Normalized Height for 0.005 m Thick Card Board.

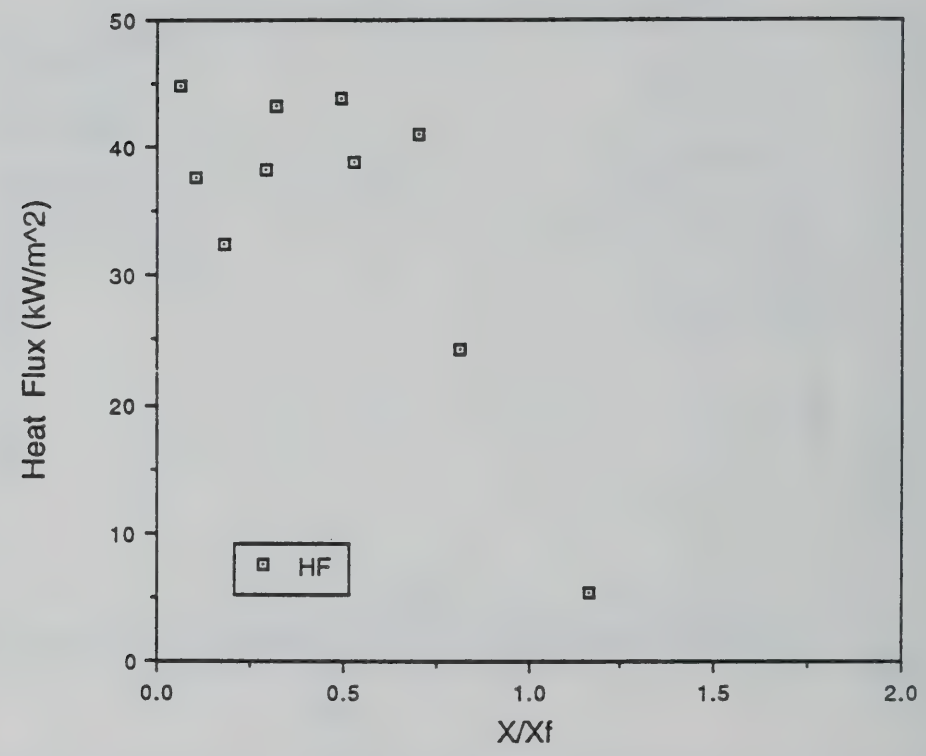

Figure 20. Total Heat Flux vs. Normalized Height for 0.0127 m Thick Polyurethane Foam.

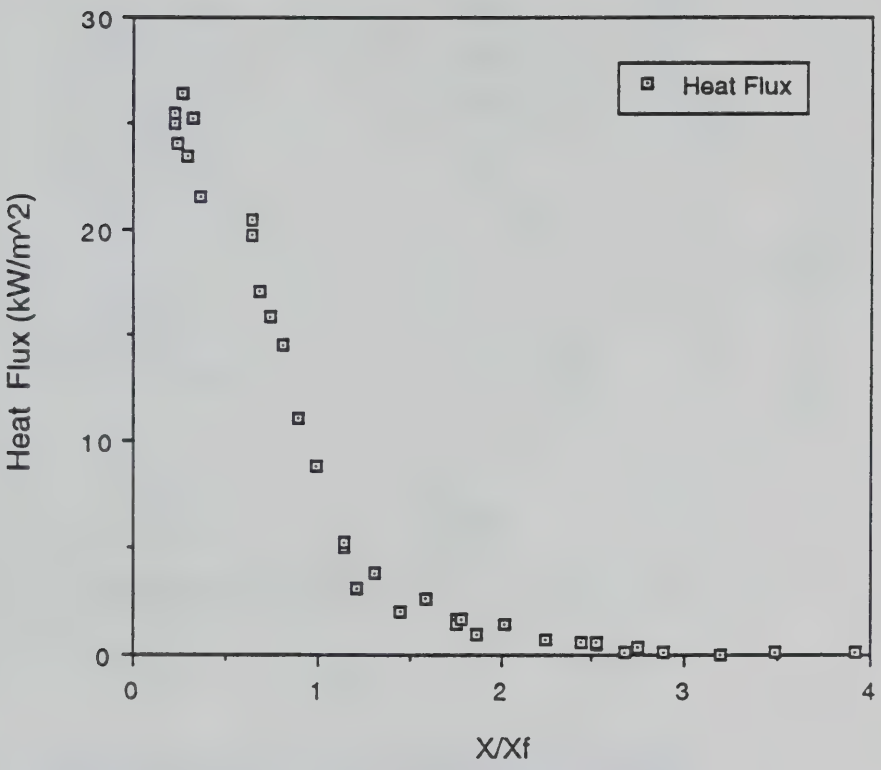

Figure 21. Total Heat Flux vs. Normalized Height for 0.0127 m Thick White Pine Board.

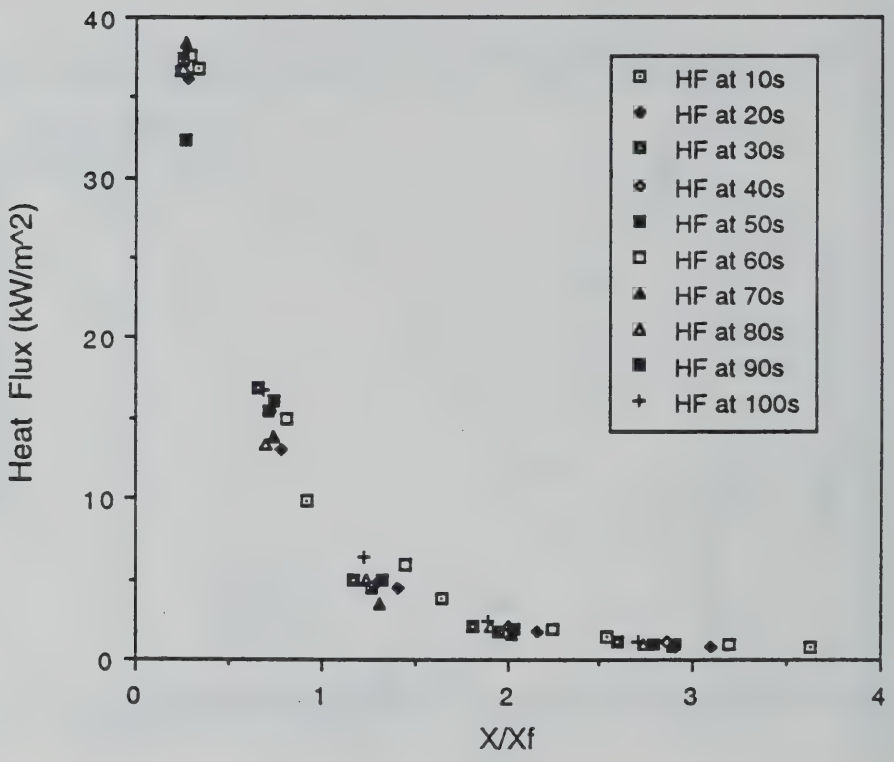

Figure 22. Total Heat Flux vs. Normalized Height for 0.0012 m Thick Red Velour Fabric.

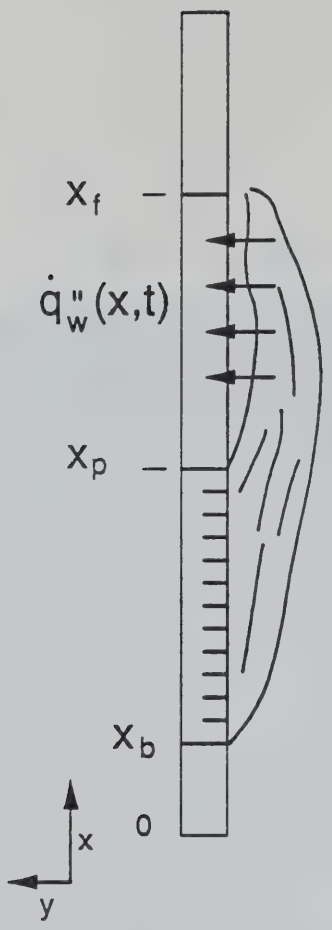

Figure 23. Schematic of upward flame spread process.

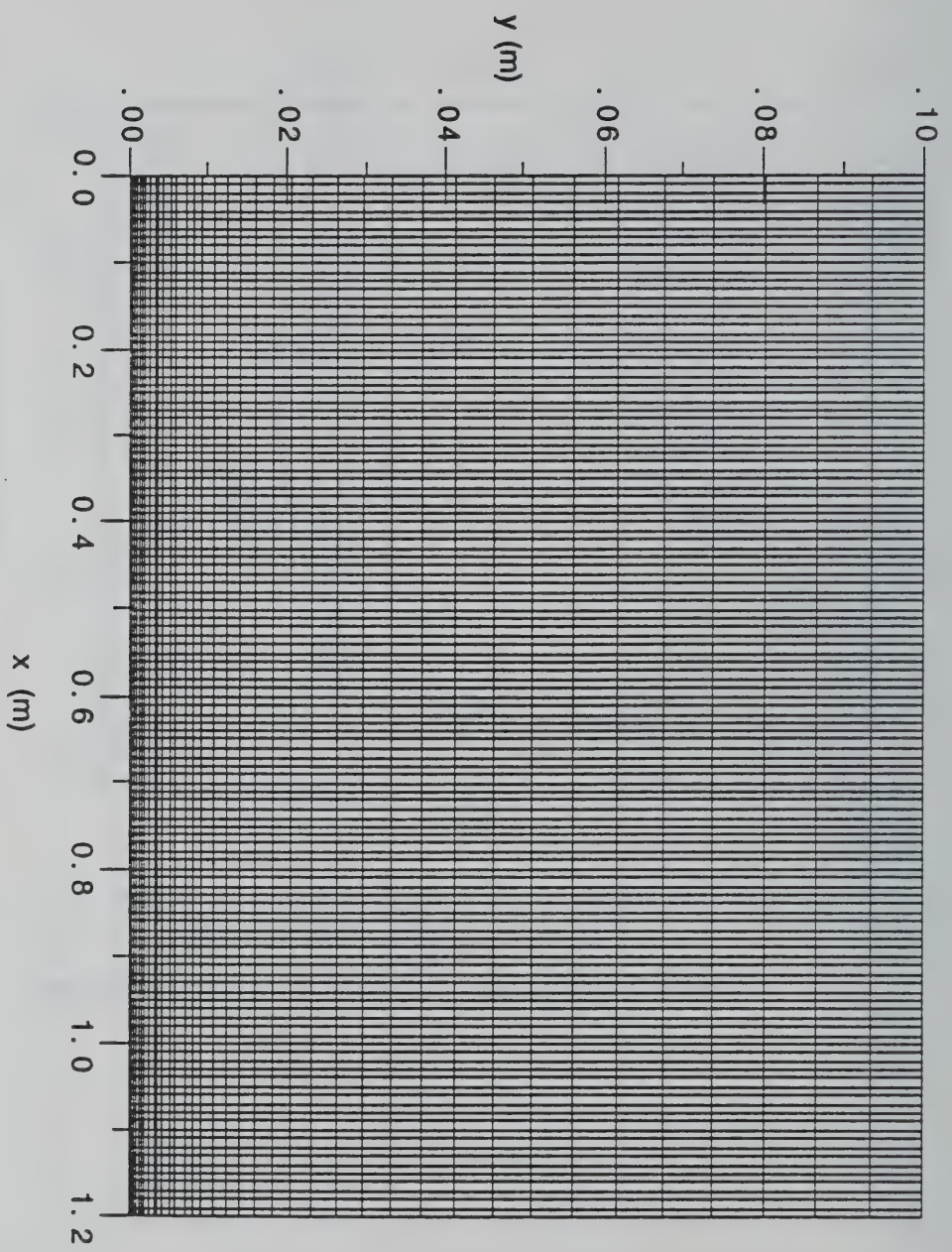

Figure 24. Node Pattern Used in Numerical Calculations.

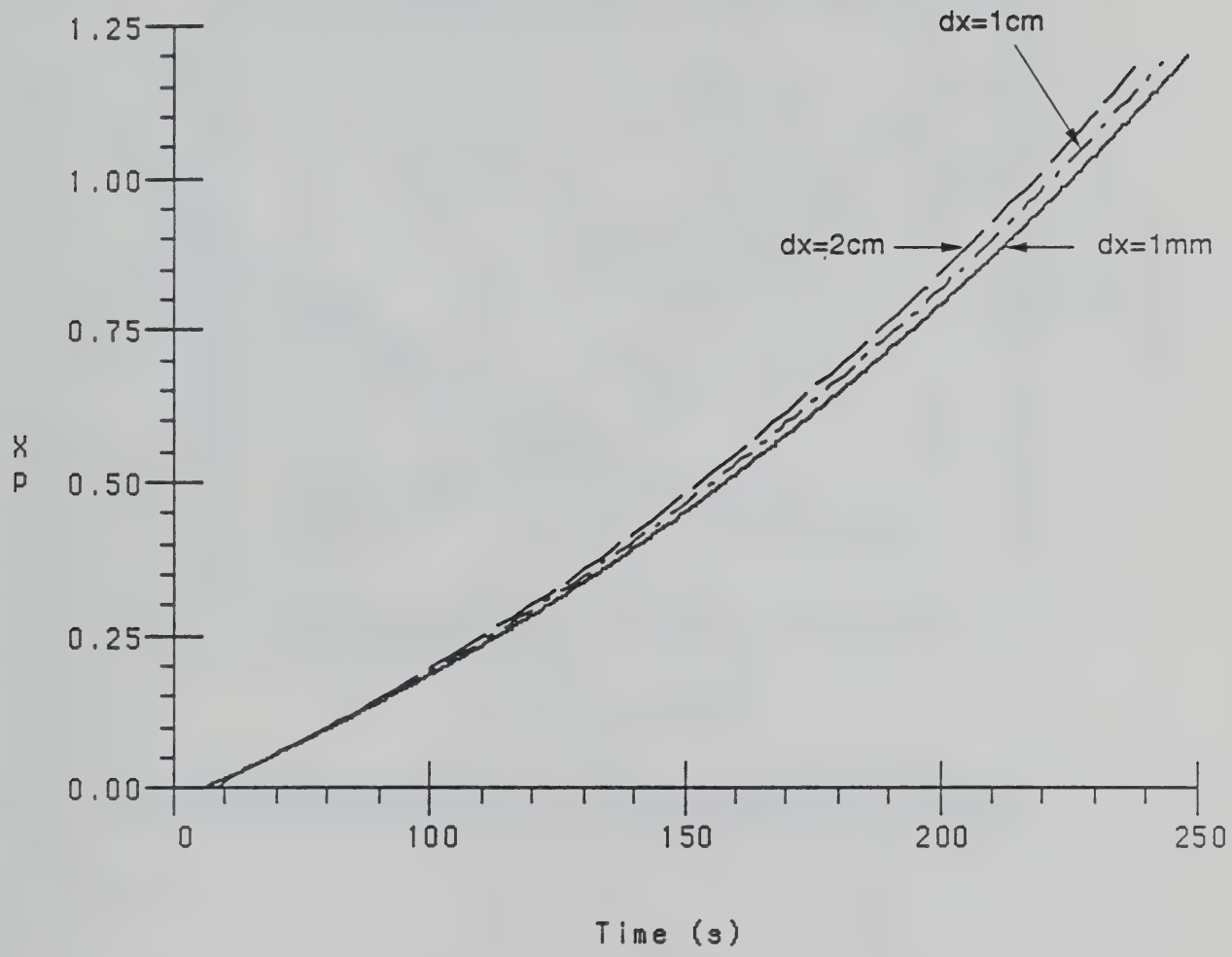

Figure 25. Effect of nodel spacing on the pyrolysis height calculation.
(1/8" clear PMMA)

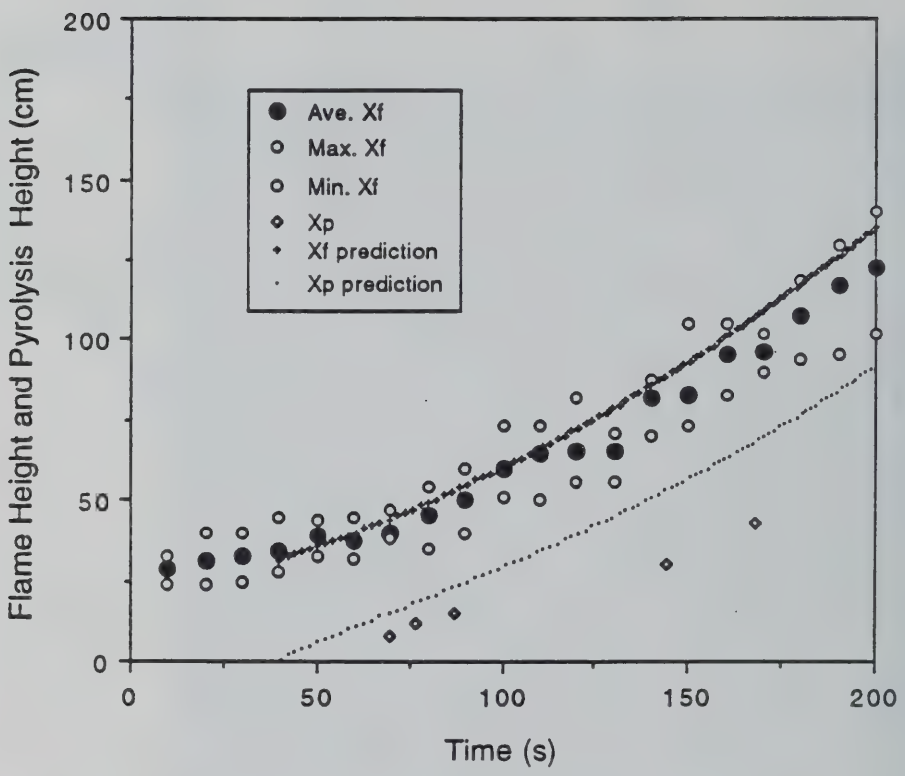

Figure 26. Prediction of Xp and Xf compared to experimental data for 3.2 mm thick PMMA slab.

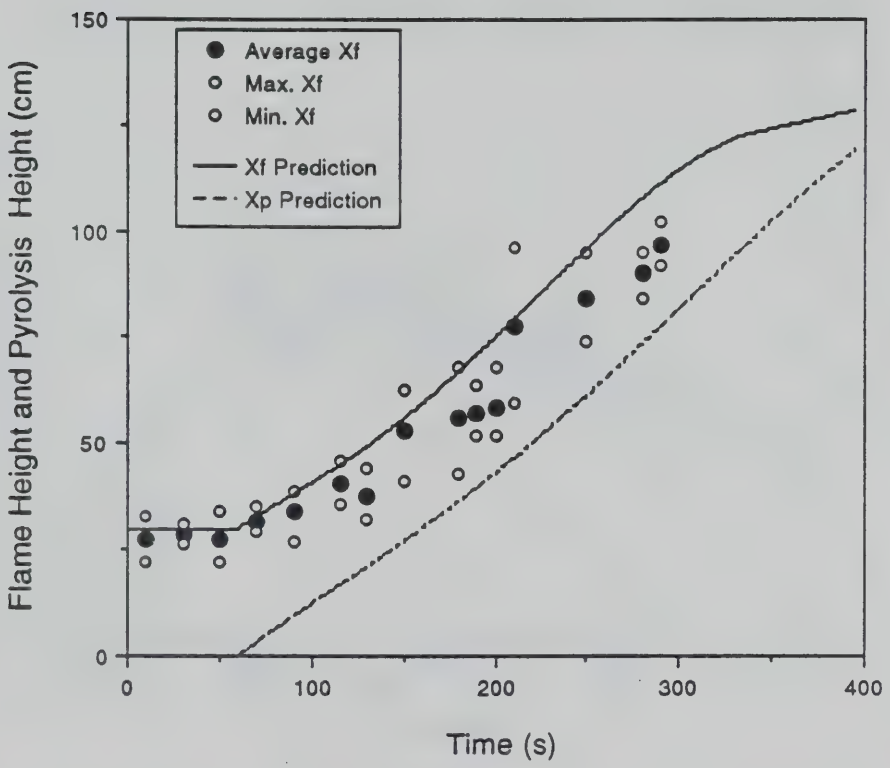

Figure 27. Prediction of Xp and Xf compared to experimental data for 3.2 mm thick masonite.

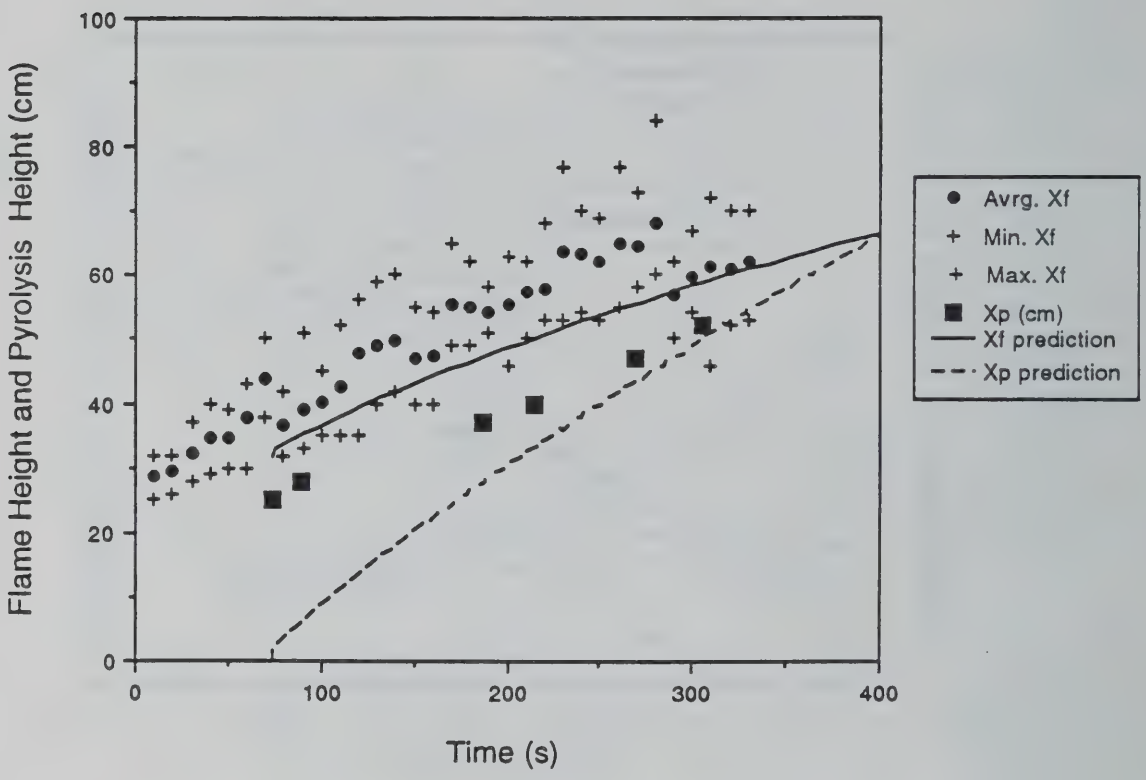

Figure 28. Prediction of Xp and Xf compared to experimental data for 5 mm thick cardboard.

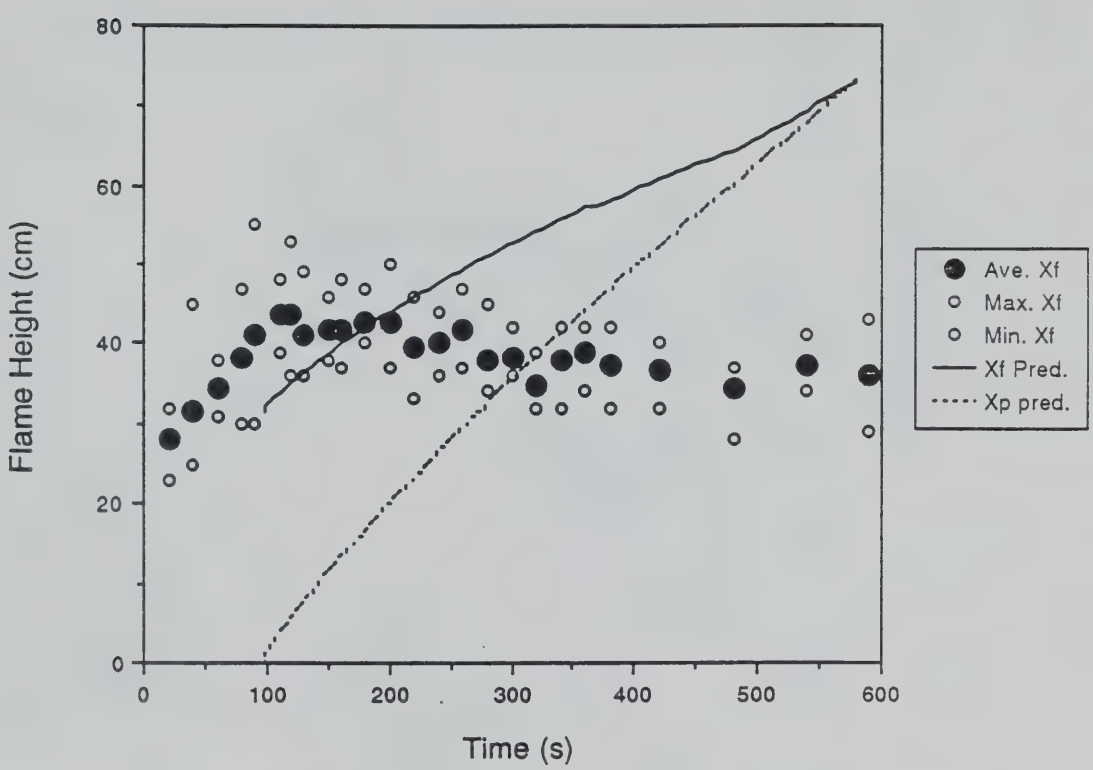

Figure 29. Measured Flame Height History Compared with Prediction for 0.0127 m Thick White Pine Board.

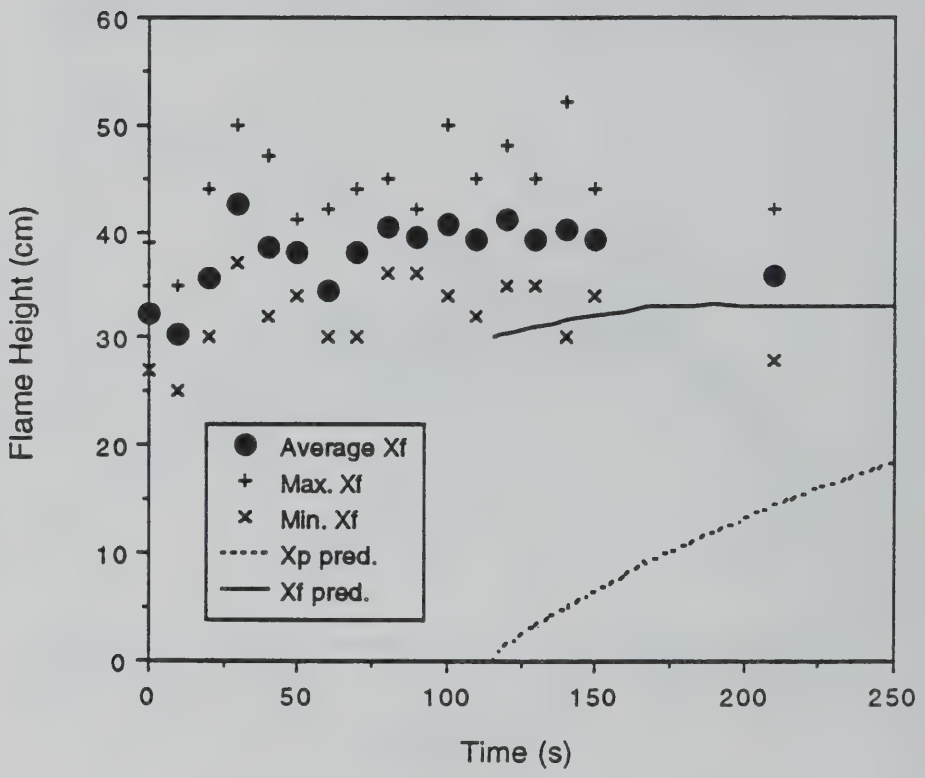

Figure 30. Measured Flame Height History Compared with Prediction for 0.0012 m Thick Red Velour Fabric.

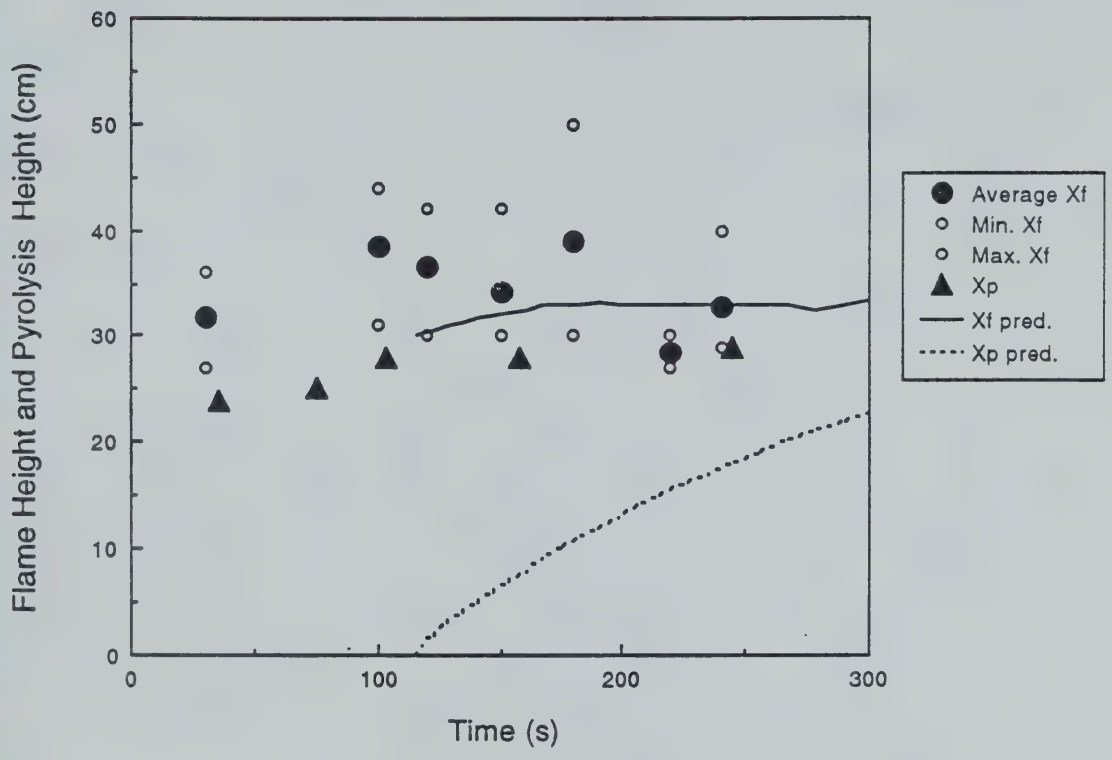

Figure 31. Measured Flame Height and Pyrolysis Height History Compared with Prediction for Velvet Polyester.

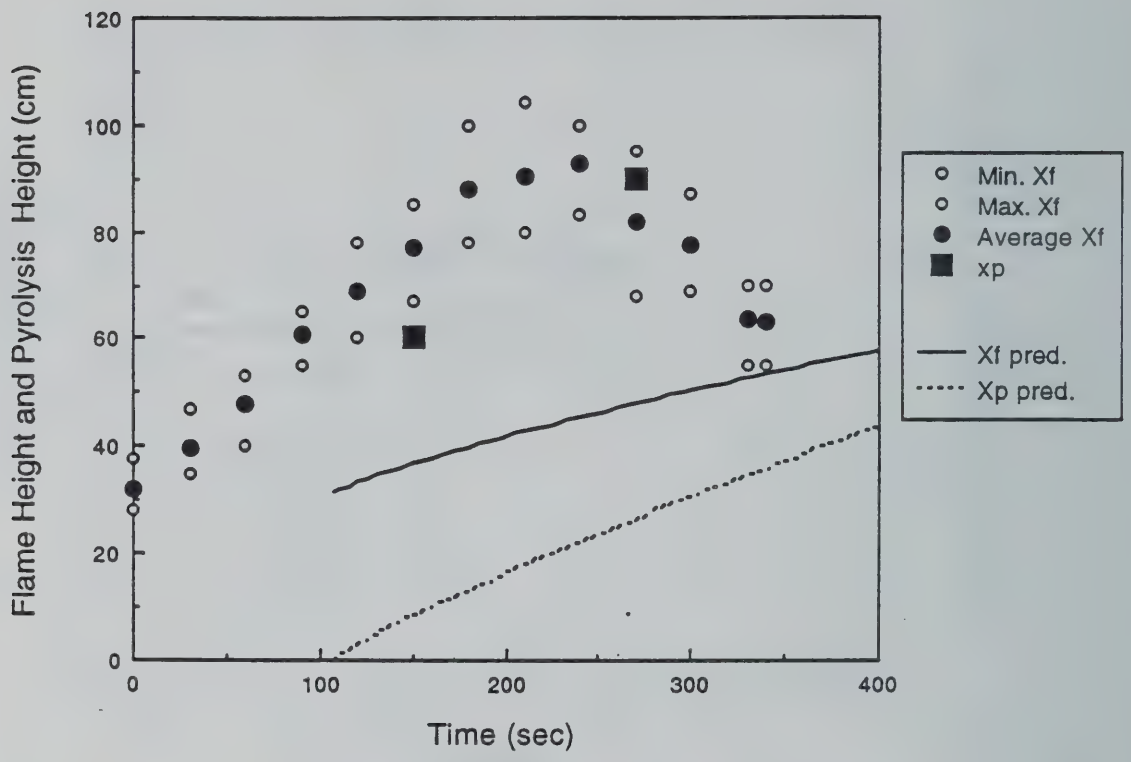

Figure 32. Measured Flame Height and Pyrolysis Height Compared with Prediction for Particle Board.

APPENDIX I

Analysis of Heat Flux Measurement by Circular Foil Gages in a Mixed Convection/Radiation Environment

This has been accepted for publication in the Journal of Heat Transfer.

ANALYSIS OF HEAT FLUX MEASUREMENT BY CIRCULAR FOIL GAGES IN A MIXED CONVECTION/RADITION ENVIRONMENT

C.H. Kuo[1] and A.K. Kulkarni[2]

Department of Mechanical Engineering
The Pennsylvania State University
University Park, PA 16802

[1] Graduate Student
[2] Associate Professor

NOMENCLATURE

h	convective heat transfer coefficient
$I_0(r)$, $I_1(r)$	Bessel's Functions of the first kind
k	thermal conductivity of the circular foil
m	$m = \sqrt{h / k\delta}$
q_c	convective heat flux per unit area to the surface (or wall)
q_g	gage-sensed heat flux per unit area
q_m	mixed (radiative and convective) heat flux per unit area to the surface (or wall) when $T_w = T_B$.
q_r	heat flux per unit area obtained from the gage output using radiation-based calibration
q_r'	radiative heat flux per unit area absorbed by the gage
q_w	total (mixed) heat flux per unit area to the surface when $T_w \neq T_B$.
r	radial coordinate of circular foil
R	radius of the circular foil
$T(r)$	temperature distribution in circular foil
T_o	temperature at the foil center
T_B	temperature of heat sink (base) which is maintained constant
T_w	surface (wall) temperature
T_∞	temperature of gas flowing over the surface
δ	thickness of foil
ΔT_r, ΔT_c, ΔT_m	temperature difference between the foil center and edge with pure radiation heat flux, pure convection heat flux, and mixed convection/radiation heat flux, respectively.

INTRODUCTION

Principles of heat flux measurement by circular foil heat flux sensors, also known as Gardon gages, are analyzed when the gages are subjected to a mixed convective/radiative heat flux. A schematic of the Gardon gage is shown in Fig. 1. The gage is constructed using a copper cylinder (usually water-cooled) with a thin constantan foil mounted on the top. A copper wire is welded at the foil center and the copper cylinder is used as the other conductor, creating a differential thermocouple between the center and the edge of the foil. The gage is mounted flush on a surface at a location where a measurement of total heat flux to the surface is desired. The heat flux incident on the constantan foil of the gage causes a temperature difference, ΔT, between the foil center and the edge which generates a corresponding voltage signal. Measurement of ΔT is then converted into the total incident

heat flux using a calibration curve or chart. Calibration is usually based on radiative heat flux, including the manufacturer-supplied calibration charts. The voltage output of the Gardon gage is almost linearly proportional to the incident heat flux when used to measure thermal radiation.

Several attempts have been made to analyze the operating principles and the error-inducing mechanisms for the circular foil heat flux sensor. Among the various effects studied are those of the transient characteristics of heat flux (Keltner and Wildin, 1975), the center wire heat loss and the heat sink temperature variation (Ash, 1969), the correction for measuring pure convection heat transfer (Borell and Diller, 1987), and the free stream velocity and its angle of attack (Young et al., 1983). The performance of Gardon gages in mixed convective-radiative environments has, however, not been investigated in depth, which is the thrust of this work.

Gardon gages are often used in the measurement of heat feedback from flames to the burning surface in a wall fire, which are exposed to a mixed heat flux consisting of comparable fractions of convection and radiation (see, for example, Saito et al.,1989). In this situation, the use of a standard calibration chart based on a purely radiative flux is questionable. Also, the gage has to be cooled to maintain a constant heat sink temperature in order to avoid melting of the junction of the foil and center wire and to provide a reference for calibration. This can cause a substantial temperature difference between the gage and the surrounding wall on which it is mounted, and introduces an error in the sensing of the convective heat flux at the location where the gage is mounted.

The specific objective of this work is to present the analysis and a methodology for estimating the *error* in the measurement of mixed convective-radiative heat flux, which is the difference between the true surface-sensed heat flux and the flux determined from the gage output using a calibration based on purely radiative heat flux.

ANALYSIS

Figure 1 helps illustrate the mathematical model used for the Gardon gage. To derive the governing equation for the temperature distribution in foil, following assumptions were employed: (i) temperature gradient across the foil thickness is negligible, (ii) heat loss from rear surface and center wire is negligible, and (iii) the convective heat transfer coefficient, h, is nearly constant on the foil. Justification of these assumptions is given by Borell and Diller (1987) and Kuo and Kulkarni (1990); the latter paper also contains more details on the present work.

The thermal diffusion equation for the foil, when exposed to a mixed convection/radiation heat flux, can be expressed as

$$\frac{d^2T}{dr^2}+\frac{1}{r}\frac{dT}{dr}+\frac{q_r'}{\delta k}+\frac{h}{\delta k}(T_\infty - T)=0 \qquad (1)$$

with two boundary conditions:

at $r = R$, $T(R) = T_B$, where T_B is the cooling water temperature;
at $r = 0$, $dT/dr = 0$.

1. Pure Radiative Heat flux

The solution of equation (1) with $h = 0$ is a second order polynomial in r, and the temperature difference between the foil center and edge is given by

$$\Delta T_r = T_O - T_B = \frac{q_r R^2}{4\delta k} \qquad (2)$$

Here, $q_r = q_r'$, ← and ΔT_r is directly related to the sensor output of the measurement. This solution has been discussed previously by Gardon (1953) and Borell and Diller (1987).

The radiation loss from the gage to the surrounding atmosphere due to its temperature *rise* from the base temperature resulting from the external heat flux is neglected here, which represents a very small fraction of q_r. If the surrounding surface has a different emissivity (and absorptivity) compared to that of the gage foil, q_r must be corrected by subtracting the term, $\sigma(\varepsilon_g - \varepsilon_w)T_w^4$, where σ is Stefan-Boltzmann constant, ε_g and ε_w are emissivities of the gage and the surrounding surface, respectively, and T_w is expressed in absolute temperature scale. However, this correction also will be small in most situations. It is assumed that the above two corrections are applied to q_r when necessary and, therefore, they are not discussed separately in the following discussion.

2. Pure Convection Heat Flux

With $q_r' = 0$, equation (1) can be rewritten as a modified Bessel's equation and its solution can be expressed in terms of the modified Bessel's function of the first kind. This case for Gardon gages was analyzed in detail by Borell and Diller (1987), therefore, only

the important results are mentioned here, which are needed later. For the center-to-edge temperature difference,

$$\Delta T_c = T_o - T_B = \frac{q_g R}{2m\delta k} \cdot \frac{I_o(mR)-1}{I_1(mR)} \equiv \frac{q_g R^2}{4\delta k} \frac{1+(mR)^2}{1+(mR)^2/2} \quad , \tag{3}$$

for small values of parameter mR, where $m = \sqrt{h/\delta k}$. Here, q_g is the average heat flux per unit area sensed by the gage foil, computed as $-k(dT/dR) \cdot 2\delta/R$ at $r = R$. (There is a typographical error in the corresponding expression of Borell and Diller [1987]). Note that ΔT_c is less than ΔT_r when $q_r = q_g$. Alternatively, if $\Delta T_c = \Delta T_r$, i.e., when the gage output is the same in pure convective and pure radiative environments, q_g is greater than q_r.

The heat transfer measurements that are usually of interest are those sensed by the *surface* or *wall*, not by the water-cooled gage. In this respect, two important points should be noted. First, the foil temperature is maximum at the center, which continuously decreases with radius to its base temperature at T = R. Therefore, local heat transfer rate on the foil varies with radius, and it has an average value of q_g over the entire foil. This needs to be corrected to the heat flux sensed by the wall in the absence of the gage, denoted by q_c. Second, the gage base temperature (T_B) is usually a fixed value because of water-cooling. If the surrounding surface temperature (T_w) is different, one more correction must be made. The case of $T_w \neq T_B$ is discussed in a later section.

The gage output gives a value of q_r when using a radiation-based calibration chart. When $T_w = T_B$, the analysis shows that

$$\frac{q_c}{q_r} = \frac{(mR/2)^2 I_o(mR)}{I_o(mR)-1} \equiv \frac{1+(mR/2)^2}{1+(mR/4)^2} \tag{4}$$

3. Mixed Heat Transfer with $T_w = T_B$

In many situations, the total heat flux to a surface has both convective and radiative components. In this case, the temperature difference between the foil center and the edge is given by

$$\Delta T_m = \left(\frac{T_B - T_\infty - q_r'/h}{I_o(mR)} + T_\infty + q_r'/h \right) - T_B = \frac{q_g R}{2m\delta k} \cdot \frac{I_o(mR)-1}{I_1(mR)} \tag{5}$$

and the average heat transfer per unit area sensed by the gage is expressed as

$$q_g = -k \cdot \frac{T_B - T_\infty - q_r'/h}{I_o(mR)} \cdot mI_1(mR) \cdot \frac{2\delta}{R} \tag{6}$$

Note that equation (5) is similar to equation (3) with a different definition of q_g. If a calibration based on radiation is used to deduce the heat flux from the measurement of ΔT_m, then ΔT_m is equated to ΔT_r, and the result is given by

$$\frac{q_g}{q_r} = \frac{mR}{2} \frac{I_1(mR)}{I_o(mR) - 1} \tag{7}$$

Finally, the wall-sensed, mixed heat transfer per unit area for $T_w = T_B$ can be expressed as

$$q_m = q_r' + h(T_\infty - T_B) = q_r \frac{(mR/2)^2 I_o(mR)}{I_o(mR) - 1} \equiv q_r \frac{1 + (mR/2)^2}{1 + (mR/4)^2} \tag{8}$$

which has a similar form to equation (4).

The ratio q_m/q_r is the correction that needs to be applied when a calibration chart based on only radiative heat flux is available. Figure 2 shows q_m/q_g, q_g/q_r and q_m/q_r ratios as a function of the parameter mR. Figure 3 shows the heat flux ratios as a function of h to further illustrate the dependence of the correction on h.

4. Mixed Heat Transfer with $T_w \neq T_B$

When T_w is not equal to T_B, an additional correction is needed to deduce wall-sensed heat transfer from the gage-sensed heat transfer. The relations for wall-sensed heat transfer (q_m) remain the same as in the case for mixed heat transfer with $T_w = T_B$, given by equation (8). The wall-sensed heat transfer with $T_w \neq T_B$ is expressed as

$$q_w = q_m + h(T_\infty - T_w) \tag{9}$$

In order to evaluate the measurement error caused by using the radiation-based calibration, q_r is compared with q_w and the following relation is obtained

$$\frac{q_r - q_w}{q_r} = \frac{q_r - q_m}{q_r} + \frac{q_m - q_w}{q_r} = 1 - \frac{(mR)^2}{4}\,\frac{I_o(mR)}{I_o(mR) - 1} + \frac{h(T_w - T_B)}{q_r} \qquad (10)$$

The value of T_w can be measured directly in experiments, and h has to be either known or estimated to obtain the correction to derive q_w from q_r. A series of curves is plotted for $\frac{q_r - q_w}{q_r}$ vs. h with parametric curves for several values of wall temperature T_w and two values of q_r in Fig. 4 using $T_B = 300$ K.

DISCUSSION

The standard calibration charts for a Gardon gage are usually prepared using a radiative heat source.* When the gage is used to measure heat flux to a surface in a mixed convective-radiative heat transfer environment, the calibration is not appropriate. This happens because the gage foil temperature is not uniform. Also, during a measurement of total heat flux to a heated surface, the gage base is normally kept at a constant temperature using cooling water, and therefore, it becomes isolated from the surrounding surface. In order to estimate the true heat flux to the surface, corrections must be applied to the heat flux that is obtained from the radiation-based calibration.

When the local wall temperature is equal to the heat sink, the error involved in the measurement of the mixed or convective heat flux is only a function of the dimensionless parameter, $mR(=\sqrt{h/k\delta}\cdot R)$. From Figs. 2 and 3, it is clear that a smaller mR value introduces a smaller error, and that the circular foil radius has a greater effect on the magnitude of error than the heat transfer coefficient according to the definition of mR itself. Therefore, a smaller diameter foil for the gage is preferable to reduce the measurement errors. The gage sensitivity, however, will be inevitably reduced due to the smaller foil diameter and the experimentalist must weigh the relative advantages of sensitivity and calibration errors which have opposite trends of dependence on the foil diameter.

Another important result revealed by the results of analysis for mixed heat transfer with $T_w = T_B$ as shown in Figs. 3 and 4 is that the correction in the measurement of mixed heat transfer using a radiation-based calibration (expressed as the ratio of q_m and q_r) *is independent of the fraction of convective heat flux in the total heat flux and it only depends on the magnitude of h.* That is, if h is fixed, the correction to be applied does not depend on whether the heat flux is predominantly convective or predominantly radiative. It may also be noted that Figs. 3 and 4 are applicable in absence of radiation, i.e., for purely convective heat flux environment.

Figure 4 shows the importance of correcting the heat flux measurement when $T_w \neq T_B$ for $T_B = 300K$. The convective heat feedback to a surface can be substantially different at higher h if the difference between T_w and T_B is large. As discussed earlier, there can be flow "tripping" if there is a large difference between T_w and T_B resulting in a different local value of h (Young et al. 1983). The experimentalist should be aware of either avoiding such a situation (for example, by keeping T_w as close to T_B as possible) or by properly accounting for the difference in local h.

Another concern here is how to estimate h for making the correction. In this situation, one may resort to a trial-and-error estimate of h in which a value of h is first assumed, the total heat flux is then derived, the convective part of it is then computed if radiative heat flux is known (or if it is zero), h is calculated based on equation $q_c = h\ (T_w - T_\infty)$, which is then compared with the first assumption, until converged. A second possibility is to estimate h independently and check for the sensitivity of the heat flux value to the variation in h and then decide whether to resort to a completely new method of heat flux measurement.

SUMMARY AND CONCLUSIONS

When a Gardon gage is used to measure convective or mixed heat flux, there is an error encountered in the measurement if the gage output is converted into heat flux using a calibration based on radiative heat flux. A theoretical analysis is presented to determine the error caused by the use of radiation-based calibration in the measurement of total heat flux that includes convective and radiative components, and in a situation where the wall temperature does not match the gage heat sink temperature. In case of mixed heat transfer, the error depends on the heat transfer coefficient *irrespective* of the magnitude of the fraction of convective heat flux in the total flux. An additional correction is necessary if the wall temperature is not the same as the base temperature. A sensor having smaller foil radius is preferable to reduce the error involved in the measurement of convective heat transfer and mixed heat transfer.

REFERENCES

Ash, R. L., 1969, "Response Characteristics of Thin Foil Heat Flux Sensors," AIAA J., Vol. 7, No. 12, pp. 2332-2335.

Borell, G. J., and Diller, T. E., 1987, "A Convection Calibration Method for Local Heat Flux Gages," J. Heat Transfer, Vol. 109, pp. 83-89.

Gardon, R., 1953, "An Instrument for Direct Measurement of Intense Thermal Radiation," Rev. Sci. Instruments, Vol. 24, No. 5, p. 366-370.

Keltner, N. R., and Wildin, M. W., 1975, "Transient Response of Circular Foil Heat Flux Gages to Radiative Fluxes," Rev. Sci. Instruments, Vol. 46, pp. 1161-1166.

Kuo, C.H. and Kulkarni, A.K., 1991, "Analysis of Heat Flux Measurement by Circular Foil Gages in a Mixed Convection/Radiation Environment," to appear in the proceedings of ASME/JSME Joint Thermal Engineering Conference, Reno, Nevada, March 17-22, 1991.

Saito, K., Williams, F. A., Wichman, I. S. and Quintiere, J. G, 1989, "Upward Turbulent Flames Spread on Wood Under External Radiation," Transaction of the ASME, J. Heat Transfer, Vol. 111, May pp. 438-445.

Young, M. F., LaRue, J.C. and Koency, J.E., "Effect of Free Velocity Vector on the Output of a Circle Disk Heat Flux Gage," ASME, Paper No. 83-HT-58, 1983.

FIGURE CAPTIONS

Fig. 1. (A) Cross-sectional view of a water-cooled Gardon gage, (B) an overall schematic, and, (C) physical model for heat transfer in the foil.

Fig. 2. Ratios of heat fluxes in the mixed convection-radiation environment as a function of the dimensionless parameter mR. The ratio q_m/q_r indicates the difference (error) between the actual heat flux incident on the surface and the heat flux indicated by the gage using radiation-based calibration for $T_w = T_B$.

Fig. 3. Ratios of the fluxes in the mixed convection-radiation environment as a function of the heat transfer coefficient for a gage having $\delta = 12.7$ μm, R = 3.11mm, k = 23 W/mK, with $T_w = T_B$.

Fig. 4. Relative difference (error) caused by using radiation-based calibration for a gage subjected to a mixed convection-radiation environment as a function of the heat transfer coefficient for two different incident radiation conditions and several values of surface temperature (T_w). Here, $T_B = 300$K, $\delta = 12.7$ μm, R = 3.11mm and k = 23 W/mK.

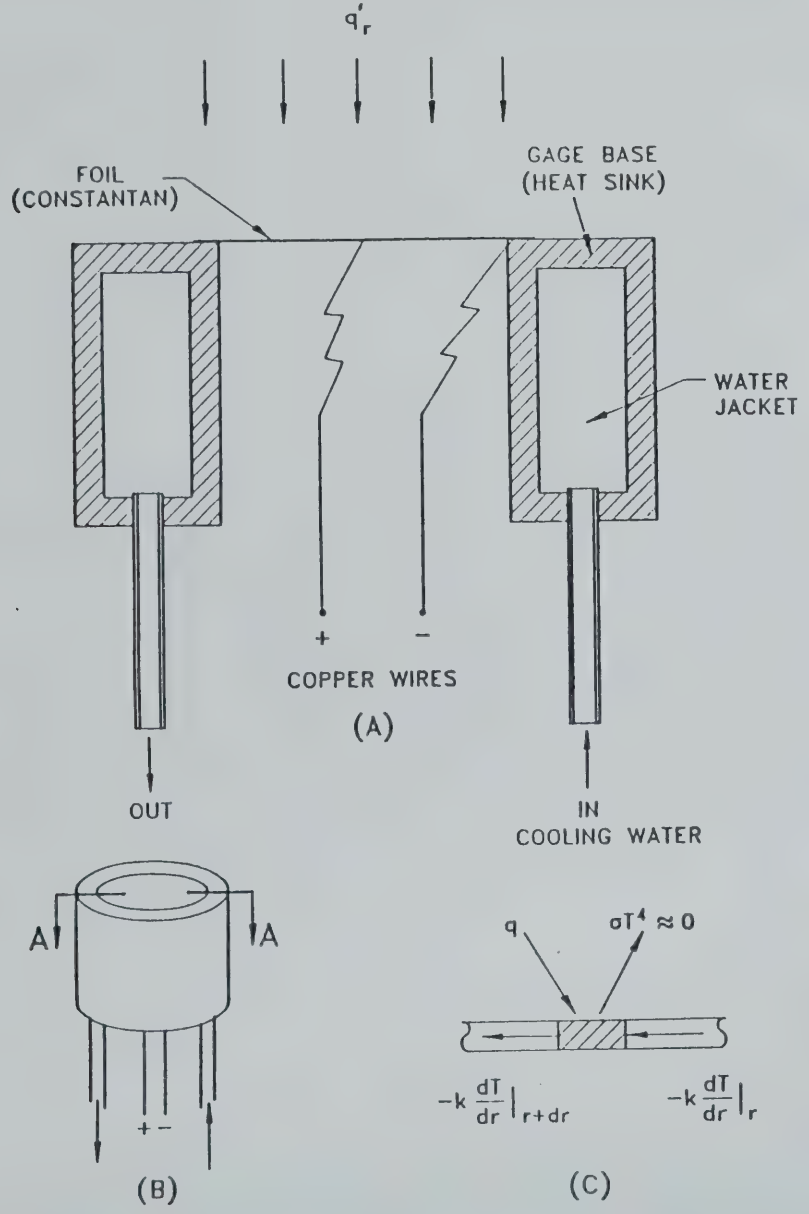

Fig. 1. (A) Cross-sectional view of a water-cooled Gardon gage, (B) Overall schematic and, (C) physical model for heat transfer in the foil.

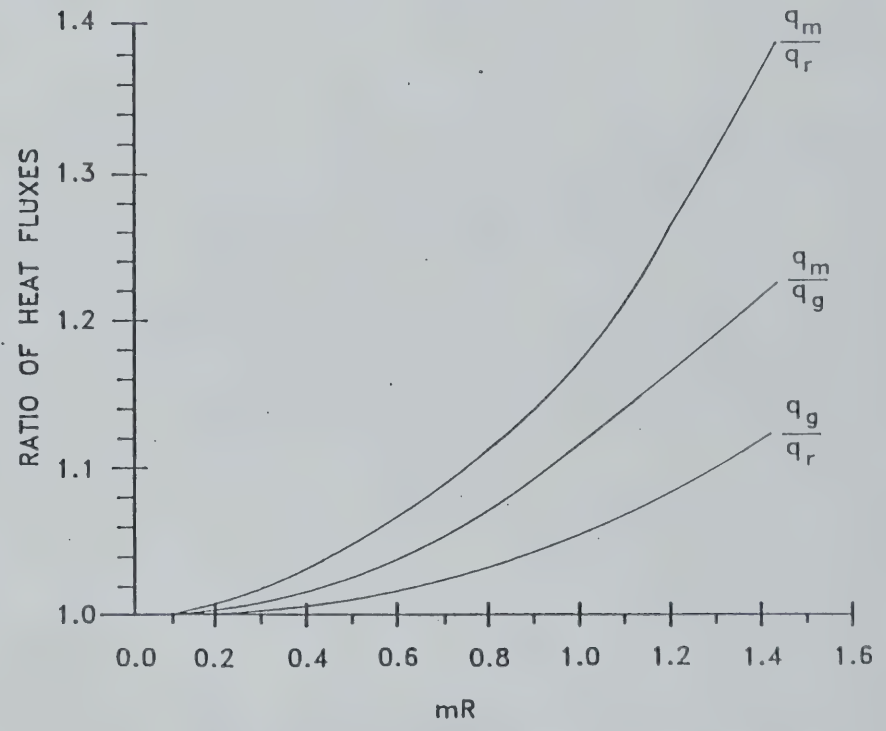

Fig. 2. Ratios of heat fluxes in the mixed convection-radiation environment as a function of the dimensionless parameter mR. The ratio q_m/q_r indicates the difference (error) between the actual heat flux incident on the surface and the heat flux indicated by the gage using radiation-based calibration for $T_w = T_B$.

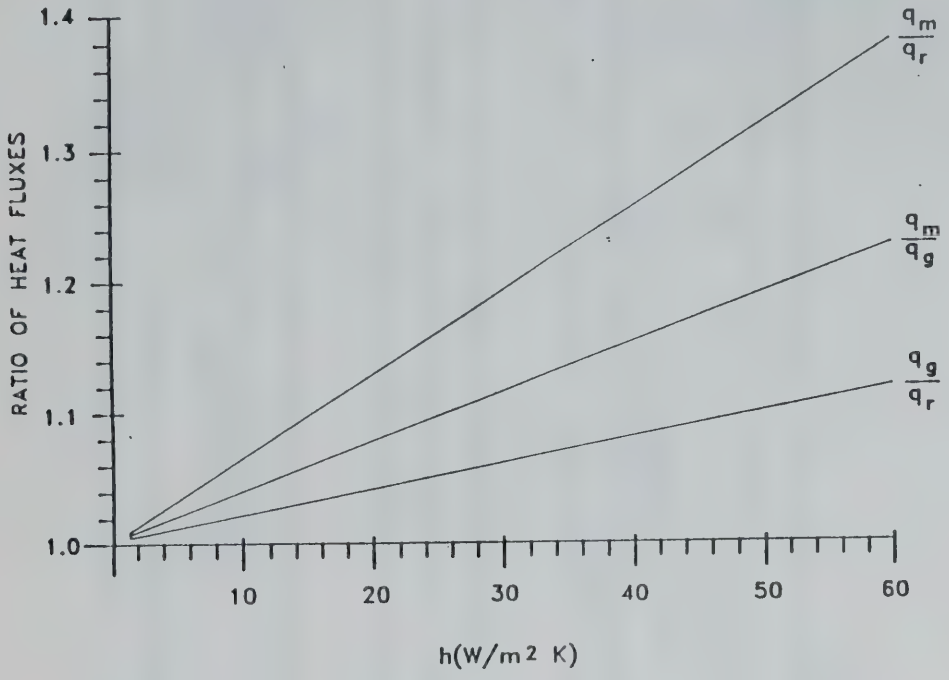

Fig. 3. Ratios of the fluxes in the mixed convection-radiation environment as a function of the heat transfer coefficient for a gage having δ = 12.7 μm, R = 3.11mm, k = 23 W/mK, with $T_w = T_B$.

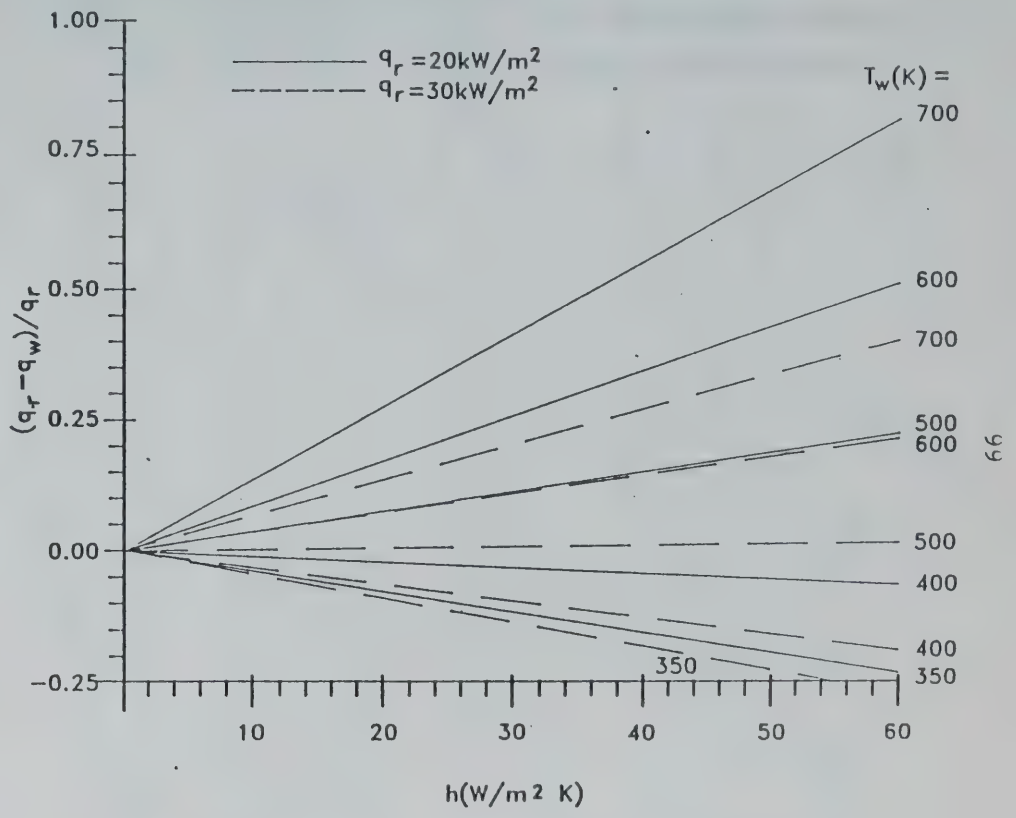

Fig. 4. Relative difference (error) caused by using radiation-based calibration for a gage subjected to a mixed convection-radiation environment as a function of the heat transfer coefficient for two different incident radiation conditions and several values of surface temperature (T_w). Here, T_B = 300 K, δ = 12.7 μm, R = 3.11mm and k = 23 W/mK.

APPENDIX II

A Generalized Correlation for Forward Heat Flux in Upward Flame Spread

Published in the Proceedings of the Eastern Section of The Combustion Institute Fall Technical Meeting, 1990

A Generalized Correlation for Forward Heat Flux in Upward Flame Spread

C. I. Kim and A. K. Kulkarni
The Pennsylvania State University
University Park, PA 16802

Introduction

It is well-established that the flame spread process depends on how fast the unburnt fuel ahead of the pyrolysis front can be heated to a critical temperature (or a range of temperatures) that causes significant pyrolysis (Figure 1). Therefore, it is essential for upward flame spread model to account the forward heat flux accurately. There have been many attempts to address the forward heat flux in upward flame spread models, starting with Thomas and Lawson [1], who assumed a constant heat feedback to the unburnt fuel ahead of pyrolysis front. Others have assumed exponential or other forms of decaying functions [2,3]. The work presented here attempts to put together the measured experimental data on the forward heat flux to correlate into a generalized correlation that can be easily applied to modeling of upward flame spread. The data covers several materials, and the correlation makes use of specially defined properties to account for the important characteristics of individual materials.

Experiments

A schematic of experimental apparatus is depicted in Figure 2. The experiment is designed to obtain flame height, pyrolysis height, burn-out height, and the forward heat flux in vertical wall fire situation. A sample with 30 cm by 120 cm is attached to 1/2" thick marinite board to emulate thin wall coverings attached to a wall construction material. Side walls and upper wall are marinite boards which prevent the flames from wrapping around the material and allow a continuous flame well above the sample height. Water-cooled, Gardon-type total heat flux gages are installed flush with the sample. Video camera with a high shutter speed is used to record the flame propagation process on tape for measuring flame height, pyrolysis height, and burn-out height at various stages of the spread. A natural gas line burner with a strength of 18 kW/m is used to ignite the samples. Heat feedback from flames was recorded as a function of time and vertical location for several different materials.

Results and Discussion

The heat feedback data, normalized with flame height and pyrolysis height, are shown in Figure 3 for various materials including results of Quintiere et al. [4]. It appears that the heat feedback data for several different materials can be collapsed in a generalized form as,

$$\dot{q}''_w(x,t) = \dot{q}''_{wo}\, g\,\{x_p(t), x_f(t), x\}$$
$$= \dot{q}''_{wo}\, exp\left[\, c_o \left(\frac{x - x_p}{x_f - x_p}\right)\right] \qquad (1)$$

where $\dot{q}''_{wo}$ is a "fire property" of the wall material, c_o is a constant, and g is a generalized function of pyrolysis height (x_p), flame tip height (x_f), and the vertical location (x). In our initial attempts of correlating the data, we assumed $\dot{q}''_{wo}$ = 25 kW/m^2 because according to the data presented by Quintiere et al. [4], the heat feedback to wall is almost constant within some scatter, i.e. $\dot{q}''_w(x)$ = 24 ± 5 kW/m^2, for all the materials they tested, upto a height 0.5 x_f, and then it drops precipitously. If $\dot{q}''_{wo}$ is fixed at 25 kW/m^2, the value of c_o for the best curvefit is –0.693. However, we later decided to estimate $\dot{q}''_{wo}$ separately for each material for two reasons, (i) it allows a more accurate correlation of $\dot{q}''_w(x,t)$, and (ii) $\dot{q}''_{wo}$ may now be treated as a material property because it more truly reflects the behavior of the material. For example, a material which has flames with greater soot concentration and has larger size flames (because of the way it pyrolyzes), has greater $\dot{q}''_{wo}$. Thus, the property $\dot{q}''_{wo}$ of the material is the heat feedback from flames to surface just above x = x_p and it is listed in Table 1 for various materials based on our measurements (except for the Douglas-Fir particle board which was based on reference [4]). Figure 4 shows normalized heat flux data with the curvefit of Equation (1).

Table 1. Characteristic Value of Forward Heat Flux.

Material	$\dot{q}''_{wo}$ (kW/m^2)
PMMA	34.6
Black PMMA	31.9
Cardboard	34.5
Douglas -Fir Particle Board	25.6

Two important points should be noted here. First, about the property $\dot{q}''_{wo}$. In our upward flame spread experiments, measurement of x_p was difficult, therefore, x_p could be measured only a few times during the flame spread with somewhat low accuracy (±10 cm). The value of $\dot{q}''_{wo}$ was then derived using interpolation at various values of x_p upto about 80 cm. We found that $\dot{q}''_{wo}$ was roughly constant with a random distribution within ±8 kW/m^2 in this range of x_p. It has been argued in the literature that, as the fire grows in size the radiative component of heat feedback increases linearly with flame height but the convective component decreases. For flame heights of upto 2.4 m, which is a typical ceiling height, the measurements of the total heat feedback does not show a significant growth with x. We, therefore, concluded that having a constant exponential factor of $\dot{q}''_{wo}$ in equation (1) is a reasonable assumption. However, it is possible to replace $\dot{q}''_{wo}$ in equation (1) by $\dot{q}''_{wo} \times f(x_p)$, where $f(x_p)$ is a function that increases with x_p and reflects the growing radiative component in the large scale fires.

The second important consideration here is the relationship between x_p and x_f. It is given by [3],

$$x_f = K \left(\dot{Q}_o' + h_c \int_0^{x_p} \dot{m}''(x)\, dx \right)^n \qquad (2)$$

where h_c is heat of combustion, $\dot{Q}_o'$ is burner strength, and $\dot{m}''(x)$ is the local mass burning rate. The variation of local burning rate with the height, x, can be obtained if the burning behavior of the material at a given location is known as a function of time, expressed as $\dot{m}''(t)$. Here, the time is measured starting with the instant at which a given location is ignited ($t = 0$), until the time at which the wall material at that location is completely burned out ($t = t_b$). The variable $\dot{m}''(t)$ thus becomes a fire property for a given wall material and, therefore, the forward heat flux $\dot{q}_w''(x,t)$ given by equation (1) automatically takes the burning behavior of that wall material into account. Details on the property $\dot{m}''(t)$ are available in reference [5]. A further investigation is necessary into both of the above-mentioned aspects.

Summary and Conclusions

Forward heat flux in upward flame spread is analyzed to yield a generalized correlation in conjunction with a fire property $\dot{q}_{wo}''$, for various practical materials listed in table 1. Heat flux data for these materials collapses nicely along the correlation. Even though this should be further verified for larger scale fire growth (in which radiation might affect the correlation) and for wider range of practical materials, results of this investigation could be incorporated into many upward flame spread models easily.

This work was supported under grant no. 60NANB8D0849 by the Center for Fire Research, National Institute of Standards and Technology, Gaithersburg, Maryland.

References

[1] Thomas, P.H., and Lawson, D.I., Joint Fire Research Organization, Fire Research Note 288, Borehamwood, U. K. (1957).

[2] Sibulkin, M. and Kim, J., Combustion Science and Technology 17, p. 39 (1977).

[3] Hasemi, Y, Fire Safety Science-Proceedings of the First International Symposium, Hemisphere Publishing Co., p. 87 (1986).

[4] Quintiere, J.G., Harkleroad, M. and Hasemi, Y., Combustion Science and Technology 48, p. 191 (1986).

[5] Kulkarni, A. K., Kim, C. I., and Mitler, H. E., Submitted for publication (1990).

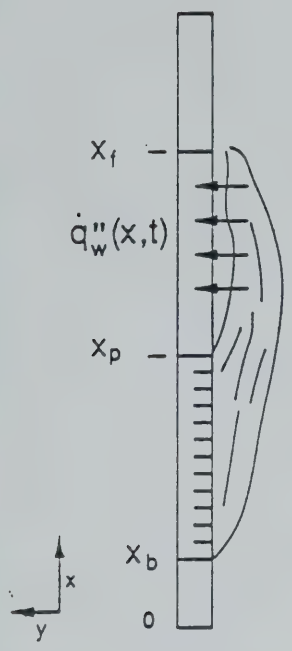

Figure 1. Schematic of upward flame spread process.

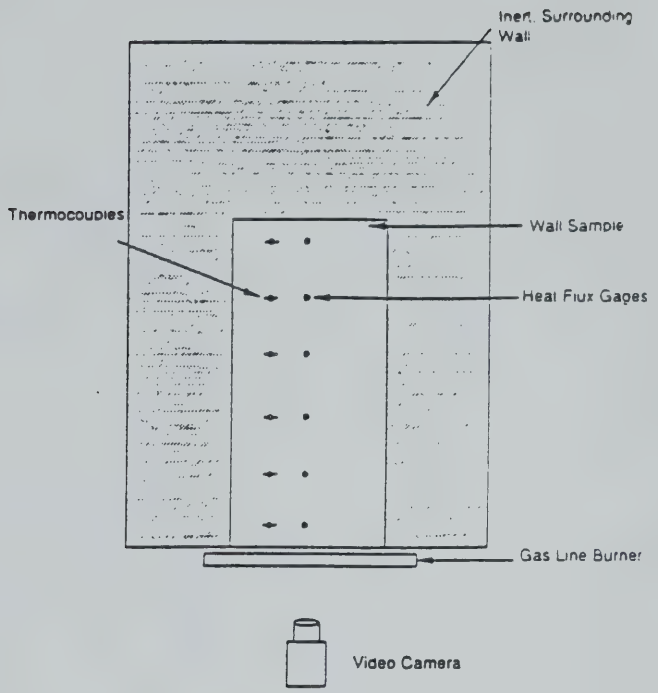

Figure 2. Schematic of experimental setup.

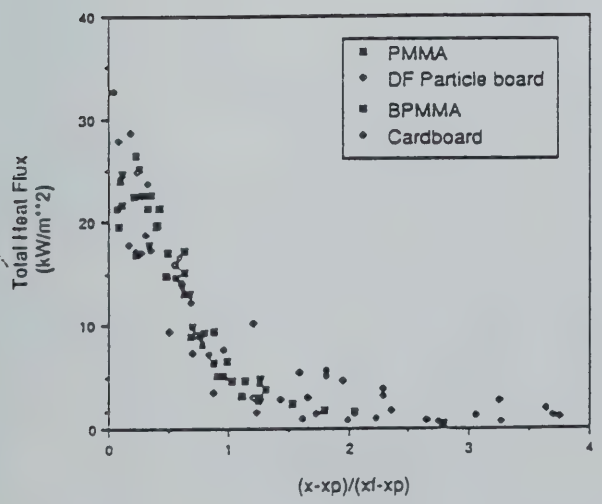

Figure 3. Total heat flux to unburnt fuel ahead of pyrolysis.

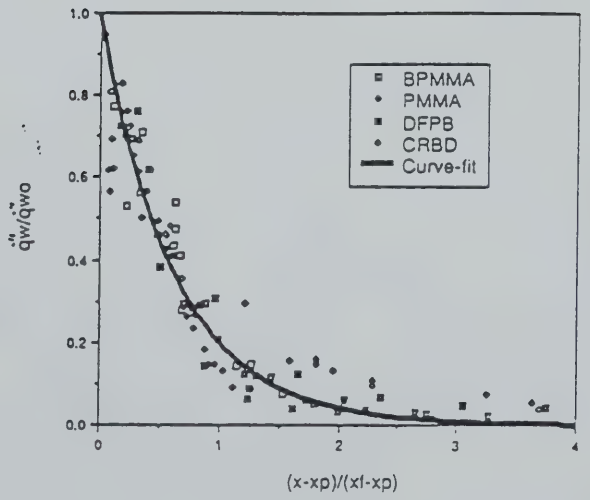

Figure 4. Normalized total heat flux with curvefit.

APPENDIX III

Time-dependent Local Mass Loss Rate of Finite-thickness Burning Wall

This section is a part of the paper by A. K. Kulkarni, C. I. Kim, and H. E. Mitler, submitted to 1991 ASME Winter Annual Meeting.

APPENDIX III

TIME -DEPENDENT LOCAL MASS LOSS RATE OF FINITE-THICKNESS BURNING WALLS

(This section is a part of a paper by A.K. Kulkarni, C.I. Kim and H.E. Mitler submitted to 1991 ASME Winter Annual Meeting.)

Introduction

The local mass loss (or burning) rate, $\dot{m}''$, of a vertical wall is an important variable in many fire-related problems, such as flame spread on a wall, fire growth and energy release rate in an enclosure fire, and the spread of smoke and hot gas plumes. For prediction of upward flame spread on a vertical wall, flame height must be calculated, which depends on the total energy release rate, which, in turn, is directly influenced by the local mass loss rate integrated over the entire pyrolyzing area of the wall. At a given location the mass loss rate is usually a strongly transient function, which depends on such factors as the external and flame heat feedback, heat conduction to the interior of the wall, material characteristics, and wall thickness. In the case of wood, for example, the burning rate peaks in the early stage of combustion due to volatile gases escaping the surface, and then tapers off as the char continues to burn. For thick polymer materials, the mass loss rate may continue to rise for an extended period due to the decreasing heat conduction to the interior. The wall thickness determines the burnout time, the time required to completely exhaust the normally combustible fraction of the wall at a given location. Thus, the local mass loss rate rises from zero at the start, goes back to zero at the burnout time, and behaves in a manner dictated by the earlier-mentioned factors, in between. It is imperative, therefore, that the local mass loss rate function $\dot{m}''(t)$, which, as explained later may be termed a "fire property" of a wall material, be known reasonably accurately for further use in other problems. The objectives of the present work were to

devise a simple small scale experiment to obtain the transient mass loss rate function $\dot{m}''(t)$ for practical wall materials.

There have been several attempts at the modeling of burning rate of wall fires (see, for example, references 1-7). Local mass loss rate for a steadily burning semi-infinite slab of fuel with laminar flames can be obtained using natural convection boundary layer theory with heat and mass transfer analogy, and with a known constant heat of vaporization [1, 2]. For turbulent wall fires, empirical correction factors for heat and mass transfer have been employed using turbulent Prandtl number and modified Reynold's analogy [3]. Orloff and others [4] proposed a correlation for local burning rate of PMMA for thermally thick turbulent wall fires. However, all these local mass loss rates were for steady state burning of vertical walls. Delichatsios and de Ris [5] proposed an expression for unsteady burning of charring fuels based on the balance of heat fluxes at the surfaces and the way the fluxes are affected by growing char layer. Delichatsios [6] also presented a method involving a more detailed system of equations for prediction of local mass loss rate of turbulent wall fires.

Recently, Mitler [7] derived an expression for $\dot{m}''(t)$ for steadily burning slabs of PMMA in a room fire situation where significant amount of external radiation heat fluxes were present with a vertical variation of room conditions due to stratification. Based on the integration of local burning rate over the entire height of pyrolysis zone, he was able to predict the total burning rate of the burning PMMA wall as a function of time which agreed very well with experiments. It has been shown that free-burning, 2 cm-thick slabs of PMMA have a strongly time-dependent mass loss rate for the first 1000 s [8]. It is clear that the local burning rate is indeed an important variable in the burning of vertical slabs which must be properly accounted for in the prediction of many fire-related phenomena. The overall purpose of the present investigation is to capture the specific behavior of materials burning in a vertical, flat surface configuration, in the form of $\dot{m}''(t)$ as a fire property of the wall material in a systematic way, using experiments.

Experiments

The primary motivation for obtaining the transient local mass loss rate was to describe the behavior of a burning vertical wall in the upward flame spreading situation where the unburnt fuel just above the pyrolysis front is continuously draped over by the flames issued by the burning region under it. Therefore, it was desirable to obtain $\dot{m}''(t)$ for a material sample under similar conditions. It has been observed experimentally [9] that the unburnt fuel above the pyrolysis front is subjected to a heat flux in the remarkably narrow range of 20 to 30 kW/m^2 by flames due to the combustion of pyrolyzed fuel coming from the burning region under the pyrolysis front. This has been observed for burning vertical walls of many different solid materials for energy release rates of 20 kW/m to 80 kW/m or a fire scale of up to approximately two meters, which is the normal room height [10]. Therefore the local, transient mass loss rate measured under the "flaming" condition, i.e. the rate measured while a small material sample is completely draped over by turbulent wall flames originating at a distance upstream, is taken to be the material fire property, to be used in analysis and for comparison purposes for most room fires. Although it is not a completely accurate description of local mass rate, it is far better than assuming a constant burning rate. This property takes into account the specific character of the material and geometry and it is only weakly dependent on the vertical location for a fire scale of about 2 m. During the upward flame spread the unburnt material just ahead of the pyrolysis front will be subjected to conditions closely similar to those present in the measurement of $\dot{m}''(t)$. An important point is that $\dot{m}''(t)$ be measured for materials as they burn in the actual case; for example, if a wall is made of a 3.2 mm masonite panel mounted on a 12.7 mm marinite (inert) substrate, it is used in the same configuration to obtain $\dot{m}''(t)$. The $\dot{m}''(t)$ thus measured can be very effectively used in fire-related models, such as upward flame spread [11].

The apparatus is shown in Figure 1. It includes an electronic balance with a digital display and analog output port, a structure made of aluminum beams, a mounting plate for the sample, a surrounding wall that covers the mounting plate, and a counterweight. A 12 cm × 12 cm

sample is first mounted on a marinite plate (in order to simulate a wall panel mounted on a dry wall) and then held flush in a larger (24 cm × 30 cm) marinite plate attached to aluminum beams. The sample is ignited with a line burner using natural gas as fuel having an energy release rate of 18 kW/m and an average flame tip height of 29 cm. The height of the burner flame is sufficient to cover the sample totally with turbulent flames because there is a clearance between the burner and the bottom of the sample. The total heat flux from burner flames to the sample location was found to be 27.5 +/- 2.5 kW/m ^{2}in the absence of the sample. The mass loss rate experiment is performed on the same day as the upward flame spread experiment for a given material and the samples for both experiments are cut from the same stock to ensure similar thermal and chemical properties of the material.

The structure between the sample and the counterweight is maintained horizontal using a level gage. The mass loss of the sample results in a change of the weight that the balance displays. The analog output of the balance is connected to an automatic data acquisition system. The electronic balance has a range of 0-500 g and has an accuracy of ±0.02 g.

Since the inert plate surrounding the sample loses weight due to drying caused by heating, and a possible slight distortion of aluminum beams may affect the data, several blank runs are made with no sample mounted, and this systematic error is corrected every time before processing the data further. Figure 2 shows the actual mass loss data for a PMMA sample and the data without any sample (blank run). The final data for the time history of the mass of the sample (the difference between the two curves in Figure 2 shown by shaded area) are fitted to a fifth order polynomial. It is differentiated and adjusted to account for the inert (pre-pyrolysis) heating period to a final form as,

$$\dot{m}''(\lambda) = \begin{cases} a_0 + a_1\lambda + a_2\lambda^2 + a_3\lambda^3 + a_4\lambda^4 & , \text{if } \lambda < \lambda_b \\ 0 , & \text{if } \lambda > \lambda_b \end{cases} \qquad (1)$$

where λ (= t -t_b) is the time measured after the beginning of pyrolysis at a specific location and λ_b is the burnout time, defined by

$$\int_0^{\lambda_b} \dot{m}''(t)\, dt = m'' \qquad (2)$$

where m'' is the combustible mass per unit area for a given sample. Because of the differentiation required on the data to obtain $\dot{m}''(t)$, the data had to be fitted with a smooth function. An examination of the data suggested a fourth or higher order polynomial; therefore, the mass loss data were fitted to a fifth order polynomial, which became a fourth order polynomial for $\dot{m}''(t)$ after differentiation.

The local mass loss rate was measured for three different materials: 3.2 mm-thick PMMA, 3.2 mm-thick masonite, and 5.0 mm-thick cardboard. Figure 3 shows the mass loss data as a function of time and the curve fits for the three materials. The mass loss rates derived from these data are given by the following expressions:

PMMA : $\dot{m}''(\lambda) = 1.723\times10^{-9} + 7.396\times10^{-5}\,\lambda - 1.551\times10^{-7}\,\lambda^2$

$- 6.566\times10^{-12}\,\lambda^3 + 1.130\times10^{-13}\,\lambda^4$, $\lambda_b = 693$ s,

Masonite : $\dot{m}''(\lambda) = 5.692\times10^{-10} + 1.011\times10^{-4}\,\lambda - 3.865\times10^{-7}\,\lambda^2$

$+ 4.811\times10^{-10}\,\lambda^3 - 1.949\times10^{-13}\,\lambda^4$, $\lambda_b = 619$ s, and

Cardboard : $\dot{m}''(\lambda) = 2.727\times10^{-3} + 1.246\times10^{-5}\,\lambda - 3.028\times10^{-8}\,\lambda^2$

$+ 2.143\times10^{-11}\,\lambda^3 - 5.048\times10^{-15}\,\lambda^4$, $\lambda_b = 1180$ s.

Figure 4 shows the mass loss rate functions for the three materials, obtained by differentiation of the mass loss polynomial curve fits.

Discussion

Figures 3 and 4 show mass loss per unit area and mass loss rate as a function of time for three different wall materials. It can be noted that the mass loss rate is far from being a constant or "steady state" value. This is especially important in case of estimating total energy release rate or for predicting upward flame spread rate on a wall. A vertical wall burns at a different rate at various locations depending on the history of ignition of the location even though the local mass rate may be completely insensitive to the actual vertical location *per se*. The instantaneous cumulative mass loss rate can then be calculated only by integrating the local mass loss rate over the entire area. The cardboard clearly burns in a very different manner compared to the other two materials. It should be noted here that the local mass loss rate function is strongly dependent on the thickness.

The experimental setup adequately simulates a burning wall with turbulent flames in a typical room fire situation because the magnitude of flame heat feedback is close to that of flames occurring in a room fire (having a scale of around 2 m). The experiments describe time dependent behavior of the local mass loss rate for practical vertical wall materials with such complexities as charring and composite structure. Thus the data obtained in this apparatus may be used as a **fire property** of the wall material for modeling purposes.

References

[1] Kosdon, F., Williams, F.A., and Buman, C., Twelfth Symposium (Int'l) on Combustion, The Combustion Institute, Pittsburgh, PA, p. 252 (1969).

[2] Kim, J., de Ris, J., and Kroesser, F.W., Thirteenth Symposium (Int'l) on Combustion, The Combustion Institute, Pittsburgh, PA, p. 949 (1971).

[3] Ahmad, T. and Faeth, G. M., Journal of Heat Transfer 100, p. 112 (1978).

[4] Orloff, L., Modak, A.T., and Alpert, R.L., Sixteenth Symposium (Int'l) on Combustion, The Combustion Institute, Pittsburgh, PA. p. 1345 (1977).

[5] Delichatsios, M. and de Ris, J., An Analytical Model of the Pyrolysis for Charring Materials, Technical Report no. 0K0J1.BU, Factory Mutual Research Corp., Norwood, MA (May, 1983).

[6] Delichatsios, M.A., Twenty-First Symposium (Int'l) on Combustion, the Combustion Institute, Pittsburgh, PA., p. 53 (1987).

[7] Mitler, H.E., Fire Safety Science, Proceedings of the Second International Symposium (Eds., C.E. Grant and P.J. Pagni), Hemisphere Publishing Co. (1988).

[8] Kim, C.I. and Kulkarni, A.K., Combustion Science and Technology vol.73, p. 493-504 (1990).

[9] Quintiere, J. G., Harkleroad, M. and Hasemi, Y., Combustion Science and Technology 48, p. 191 (1986).

[10] Quintiere, J.G., Journal of Research of the National Bureau of Standards 93, p. 61 (1988).

[11] Kim, C.I. and Kulkarni, A.K., Submitted to Fire Safety Science (1990).

[12] Steckler, K.D. and Mitler, H.E., Proceedings of the Fall Technical Meeting of The Eastern Section of The Combustion Institute, Clearwater Beach, Florida, p. 73-1(December 1988).

[13] Kashiwagi, T. and Ohlemiller, T.J., 19th Symposium (Int'l) on Combustion, the Combustion Institute, Pittsburgh, PA., p. 815 (1982).

NIST-114A
(REV. 3-90)

U.S. DEPARTMENT OF COMMERCE
NATIONAL INSTITUTE OF STANDARDS AND TECHNOLOGY

BIBLIOGRAPHIC DATA SHEET

1. PUBLICATION OR REPORT NUMBER
NIST-GCR-91-597

2. PERFORMING ORGANIZATION REPORT NUMBER

3. PUBLICATION DATE
September 1991

4. TITLE AND SUBTITLE

Turbulent Upward Flame Spread for Burning Vertical Walls Made of Finite Thickness

5. AUTHOR(S)

A.K. Kulkarni, C.I. Kim and C.H. Kuo

6. PERFORMING ORGANIZATION (IF JOINT OR OTHER THAN NIST, SEE INSTRUCTIONS)
Pennsylvania State University
Department of Mechanical Engineering
University Park, PA 16802

7. CONTRACT/GRANT NUMBER
NIST Grant No. 60NANB8D0849

8. TYPE OF REPORT AND PERIOD COVERED
Annual Report 8/15/89-8/14/90

9. SPONSORING ORGANIZATION NAME AND COMPLETE ADDRESS (STREET, CITY, STATE, ZIP)
U.S. Department of Commerce
National Institute of Standards & Technology
Gaithersburg, MD 20899

10. SUPPLEMENTARY NOTES

11. ABSTRACT (A 200-WORD OR LESS FACTUAL SUMMARY OF MOST SIGNIFICANT INFORMATION. IF DOCUMENT INCLUDES A SIGNIFICANT BIBLIOGRAPHY OR LITERATURE SURVEY, MENTION IT HERE.)

Progress made during the second year of the NIST grant number 60NANB8D0849 for the period August 15, 1989 through August 14, 1990 is reported here. This report marks the end of the first phase of the grant, for which the overall objective was to understand the basic mechanisms of upward flame spread and to develop a complete procedure to predict the flame spread on practical wall materials of finite thickness, appropriately vertified by experiments. These objectives have been met. Specifically in the past year, several wall materials were tested in the upward flame spread apparatus, mathematical model development for predicting the upward flame spread was completed, and comparisons of data and predictions were made, in addition to completion of many other supporting tasks.

12. KEY WORDS (6 TO 12 ENTRIES; ALPHABETICAL ORDER; CAPITALIZE ONLY PROPER NAMES; AND SEPARATE KEY WORDS BY SEMICOLONS)
flame spread; masonite (trademark); mathematical models; polymethylmethacrylate; polyurethane foams; pyrolysis; textiles; wall fires; wood

13. AVAILABILITY

X	UNLIMITED
	FOR OFFICIAL DISTRIBUTION. DO NOT RELEASE TO NATIONAL TECHNICAL INFORMATION SERVICE (NTIS).
	ORDER FROM SUPERINTENDENT OF DOCUMENTS, U.S. GOVERNMENT PRINTING OFFICE, WASHINGTON, DC 20402.
X	ORDER FROM NATIONAL TECHNICAL INFORMATION SERVICE (NTIS), SPRINGFIELD, VA 22161.

14. NUMBER OF PRINTED PAGES
88

15. PRICE
A05

ELECTRONIC FORM